Structure

The structure-function relationship of a signaling-competent, dimeric Reelin fragment

Graphical abstract

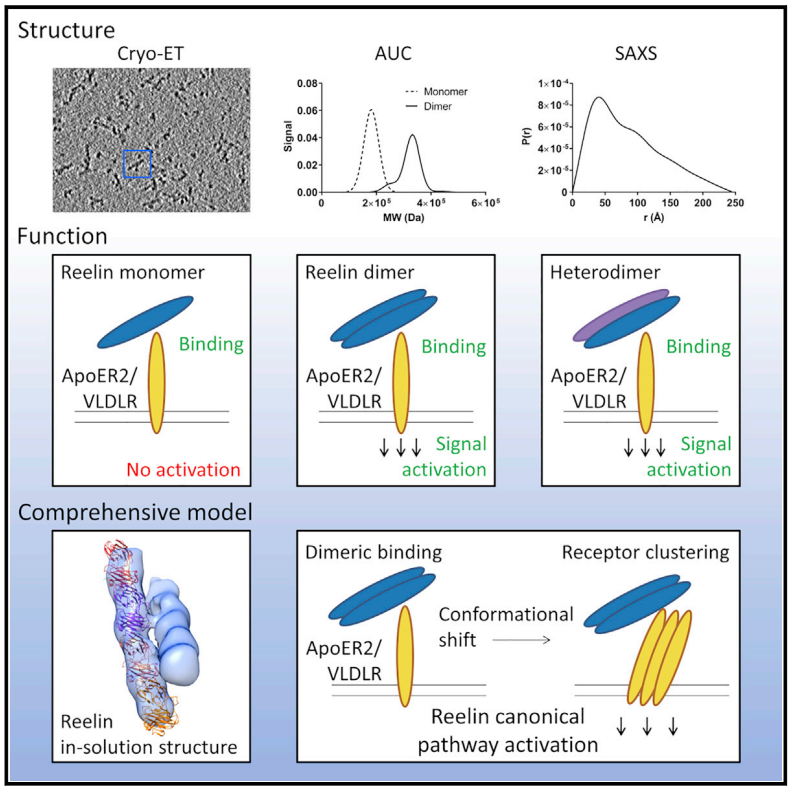

Highlights

- Cryo-ET reveals the architecture of a dimeric, signaling-competent Reelin fragment
- Biophysical data confirm the structure and detail of Reelin's oligomerization state
- A Reelin heterodimer initiates signal activation in dissociated neurons
- Data support a canonical pathway activation model that relies on dimeric conformation

Authors

Liam S. Turk, Xuyuan Kuang, Valentina Dal Pozzo, ..., Gabriella D'Arcangelo, Wei Dai, Davide Comoletti

Correspondence

wei.dai@rutgers.edu (W.D.), davide.comoletti@vuw.ac.nz (D.C.)

In brief

Several aspects of brain development and function are reliant on the secreted glycoprotein Reelin. Turk et al. characterize the binding and signaling properties of a variety of Reelin fragments. The authors also present the in-solution structure of Reelin's dimeric central fragment and propose a structure-informed model of signal activation.

Turk et al., 2021, Structure 29, 1–15
October 7, 2021
https://doi.org/10.1016/j.str.2021.05.012

Please cite this article in press as: Turk et al., The structure-function relationship of a signaling-competent, dimeric Reelin fragment, Structure (2021), https://doi.org/10.1016/j.str.2021.05.012

Structure

CellPress

Article

The structure-function relationship of a signaling-competent, dimeric Reelin fragment

Liam S. Turk,[1,2,3] Xuyuan Kuang,[4,5,6] Valentina Dal Pozzo,[4] Khush Patel,[4] Muyuan Chen,[7] Kevin Huynh,[4,5] Michael J. Currie,[8] Daniel Mitchell,[3] Renwick C.J. Dobson,[8,9] Gabriella D'Arcangelo,[4] Wei Dai,[4,5,*] and Davide Comoletti[1,2,3,10,*]

[1]Child Health Institute of New Jersey, New Brunswick, NJ 08901, USA
[2]Department of Neuroscience and Cell Biology, Robert Wood Johnson Medical School, Rutgers, The State University of New Jersey, New Brunswick, NJ 08901, USA
[3]School of Biological Sciences, Victoria University of Wellington, Wellington 6012, New Zealand
[4]Department of Cell Biology and Neuroscience, Rutgers, The State University of New Jersey, Piscataway, NJ 08854, USA
[5]Institute for Quantitative Biomedicine, Rutgers, The State University of New Jersey, Piscataway, NJ 08854, USA
[6]Department of Hyperbaric Oxygen, Central South University, Changsha, Hunan Province, China
[7]Verna and Marrs McLean Department of Biochemistry and Molecular Biology, Baylor College of Medicine, Houston, TX 77030, USA
[8]Biomolecular Interactions Centre and School of Biological Sciences, University of Canterbury, Christchurch 8041, New Zealand
[9]Bio21 Molecular Science and Biotechnology Institute, Department of Biochemistry and Molecular Biology, University of Melbourne, Parkville, VIC 3010, Australia
[10]Lead contact
*Correspondence: wei.dai@rutgers.edu (W.D.), davide.comoletti@vuw.ac.nz (D.C.)
https://doi.org/10.1016/j.str.2021.05.012

SUMMARY

Reelin operates through canonical and non-canonical pathways that mediate several aspects of brain development and function. Reelin's dimeric central fragment (CF), generated through proteolytic cleavage, is required for the lipoprotein-receptor-dependent canonical pathway activation. Here, we analyze the signaling properties of a variety of Reelin fragments and measure the differential binding affinities of monomeric and dimeric CF fragments to lipoprotein receptors to investigate the mode of canonical signal activation. We also present the cryoelectron tomography-solved dimeric structure of Reelin CF and support it using several other biophysical techniques. Our findings suggest that Reelin CF forms a covalent parallel dimer with some degree of flexibility between the two protein chains. As a result of this conformation, Reelin binds to lipoprotein receptors in a manner inaccessible to its monomeric form and is capable of stimulating canonical pathway signaling.

INTRODUCTION

Reelin is a critical player in brain development and function, and its loss in mutant *reeler* mice results in the massive disruption of cortical cellular layers, cerebellar hypoplasia, and severe ataxia (D'Arcangelo et al., 1995). This large (~400 kDa) glycoprotein is secreted by Cajal-Retzius cells and a subset of GABAergic interneurons to regulate many aspects of pre- and postnatal brain development (Lee and D'Arcangelo, 2016). Specifically, Reelin cues the radial migration of principal neurons to form laminated cortical brain structures, promotes the growth and orientation of dendritic arbors, induces the branching of entorhinohippocampal axon terminals, induces spine formation, and modulates synaptic function and plasticity, affecting learning and memory (Borrell et al., 1999; Del Rio et al., 1997; Iafrati et al., 2014; Lambert de Rouvroit and Goffinet, 1998; Liu et al., 2001; Matsuki et al., 2010; Nichols and Olson, 2010; Niu et al., 2004, 2008; Olson et al., 2006; Qiu et al., 2006; Rice et al., 2001; Weeber et al., 2002).

Structurally, Reelin is a multi-domain protein consisting of N-terminal F-spondin-like and H domains, eight Reelin repeat domains (RRs), and a short C-terminal stretch of basic amino acids (D'Arcangelo et al., 1995). Full-length (FL) Reelin, secreted by Cajal-Retzius cells in the embryonic brain, forms oligomers that accumulate in the marginal zone and control neuronal migration (Kubo et al., 2002; Ogawa et al., 1995). Some Reelin proteins, however, are cleaved by metalloproteases in what may be a form of activity regulation, resulting in three major products, the N-terminal fragment (NT), the central fragment (CF), and the C-terminal fragment (CT) (Figures 1 and S1) (D'Arcangelo et al., 1997; Koie et al., 2014; Lambert de Rouvroit et al., 1999; Ogino et al., 2017; Sato et al., 2016). It has been reported that Reelin CF is necessary and sufficient to elicit signal transduction in dissociated neurons (Jossin et al., 2004). Furthermore, to be functionally active, Reelin must form a covalent homodimer mediated by a disulfide bond that bridges one cysteine residue (C2101) on repeat 5 with its intermolecular counterpart. The mutant Reelin C2101A is unable to form a disulfide-linked dimer and can no longer efficiently activate Reelin signaling, yet it retains the ability to bind to Reelin's receptors (Yasui et al., 2011).

Reelin exerts its biological functions primarily through the activation of a canonical signaling pathway, in which Reelin binds to either of its two known receptors in the lipoprotein receptor superfamily, the very low density lipoprotein receptor (VLDLR) and apolipoprotein E receptor 2 (ApoER2) (D'Arcangelo et al.,

Please cite this article in press as: Turk et al., The structure-function relationship of a signaling-competent, dimeric Reelin fragment, Structure (2021), https://doi.org/10.1016/j.str.2021.05.012

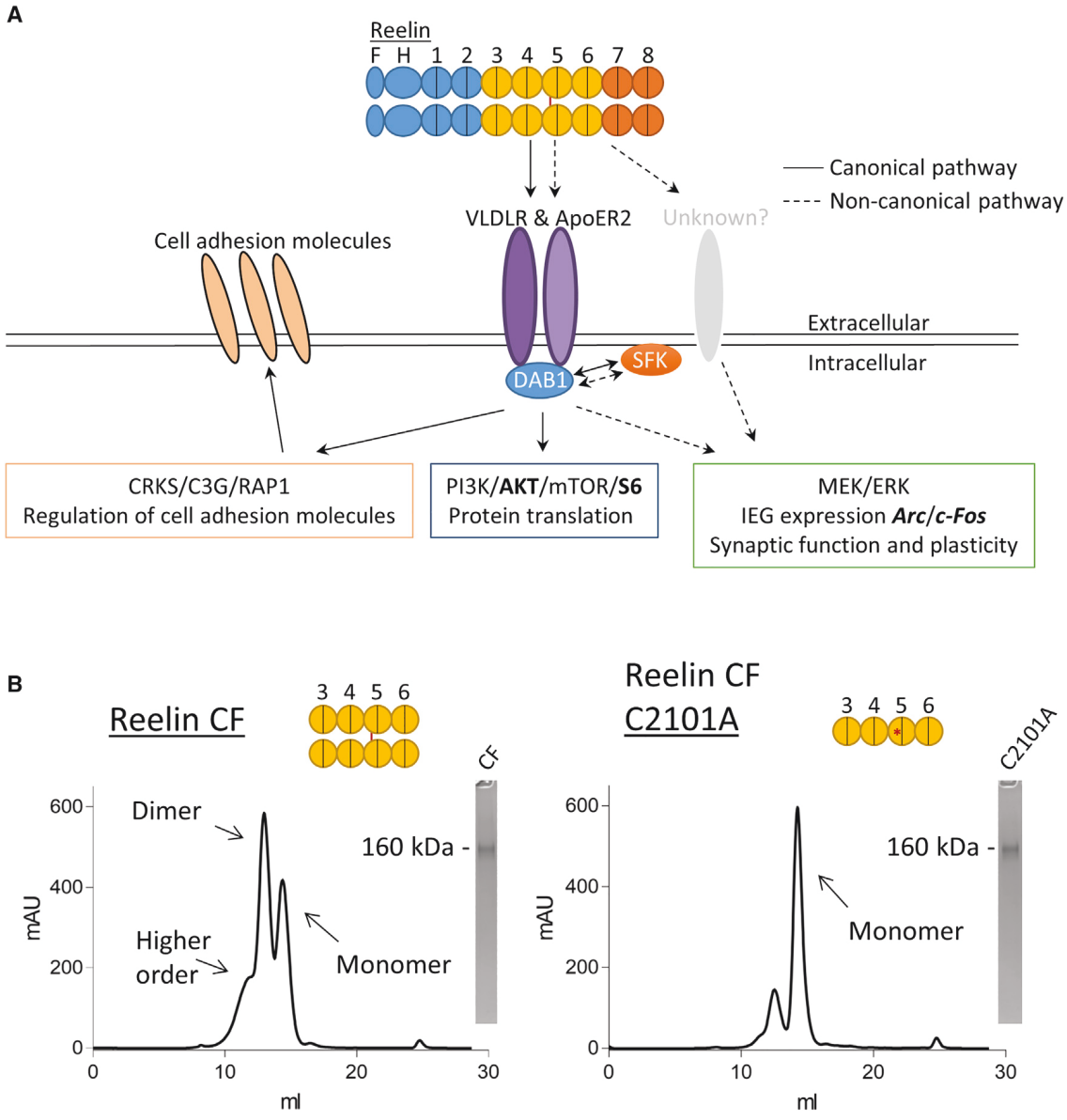

Figure 1. Expression and purification of Reelin proteins

(A) Diagram of Reelin signaling pathways. In bold are the downstream signaling molecules analyzed in this study.

(B) Diagrams, SEC traces, and SDS-PAGE under reducing conditions followed by Coomassie staining of purified Reelin CF constructs (left, CF; right, CF C2101A). For Reelin CF, the dimeric peak elutes at ~13 mL, and the monomeric peak elutes at ~14.25 mL. Reelin CF C2101A elutes primarily as a peak at ~14.25 mL. The oligomeric state of each species is confirmed later in the study by AUC (Figures 7 and S8).

1999; Hiesberger et al., 1999). Reelin binding to these receptors leads to the phosphorylation of the adaptor protein Dab1 by Src-family kinases (SFKs) and downstream activation of the growth-regulating PI3K/Akt/mTOR signaling pathway (Bock et al., 2003; D'Arcangelo et al., 1999; Dlugosz et al., 2019; Howell et al., 1999; Jossin and Goffinet, 2007; Park and Curran, 2008). Reelin also activates a non-canonical pathway, leading to the SFK-dependent phosphorylation of Erk1/2 kinases and the expression of synaptic immediate-early genes (IEGs) through mechanisms that are not well characterized (Lee et al., 2014).

Reelin's large size, dimeric composition, complex cleavage pattern, and multiple repeat domain organization have made structural studies of the protein difficult to conduct. Whereas the structures of some individual domains and domain pairs have been solved by protein crystallography (Nagae et al., 2020; Nogi et al., 2006; Yasui et al., 2007; Yasui et al., 2010), the structure of a signaling-competent Reelin fragment, which we define as its dimeric CF, has thus far remained unresolved.

Here we present a multidisciplinary study that investigates the Reelin structure-function relationship. Our findings demonstrate that, unlike the proteolytic fragments examined here, only Reelin FL robustly activates both the canonical and the non-canonical pathways. Furthermore, we show that the CF dimer is sufficient to activate the canonical Reelin signaling pathway, whereas the

Please cite this article in press as: Turk et al., The structure-function relationship of a signaling-competent, dimeric Reelin fragment, Structure (2021), https://doi.org/10.1016/j.str.2021.05.012

CF monomer and other Reelin fragments are not. We calculate the dissociation constants (K_D) between the dimeric and the monomeric fragments of Reelin and the receptors, VLDLR and ApoER2. We also report the in-solution structure of the signaling-competent dimeric CF, obtained using cryoelectron tomography (cryo-ET). We confirm the architecture of the monomeric fragment using small-angle X-ray scattering (SAXS), as an independent, in-solution technique, and assess the dimerization behavior using analytical ultracentrifugation (AUC). Last, by incorporating a Reelin CF heterodimer into our signaling assay, we present a model of canonical signal activation that highlights the importance of Reelin's dimeric structure.

RESULTS

Preparation of purified Reelin fragments

We generated and purified a series of Reelin constructs corresponding to Reelin FL and the three major cleavage products (Reelin NT, CF, and CT) to investigate their canonical and non-canonical signaling properties. Reelin CF was also purified as a dimeric Fc-fusion protein (CF-Fc) and mutant monomeric version (CF C2101A) (Figures 1 and S1). The purity and integrity of the purified Reelin proteins used in these experiments were routinely verified by size-exclusion chromatography (SEC) and/or SDS-PAGE followed by Coomassie stain (Figures 1B and S1). Reelin CF eluted as three distinct products in SEC, which we term higher order, dimer, and monomer, and the biophysical properties of these oligomeric states are further investigated later in this study using AUC. It is unsurprising that the Reelin CF construct purifies partially as a monomer due to the inclusion of 1 mM DTT in the purification buffer, thus leading to the partial reduction of the C2101 disulfide bond, responsible for maintaining the Reelin CF dimer. Reelin CF C2101A eluted primarily as a peak that corresponds in elution volume to the monomeric peak observed for Reelin CF (Figure 1B). The minor peak observed in the Reelin CF C2101A SEC trace is likely an artifactual dimer, and biophysical properties of this construct are investigated later in the study as well. Constructs expressed and purified as Fc-fusion proteins (i.e., Reelin CF-Fc, Reelin CF K2467A-Fc) often run as double bands due to the partial cleavage of the Fc during protein preparation (Figure S1). Reelin CT eluted as a single, uniform peak in SEC, but consistently ran as three distinct bands in SDS-PAGE (~85, ~65, and ~20 kDa), which we attribute to partial degradation as a result of denaturation or reduction prior to SDS-PAGE (Figure S1).

Reelin FL and CF dimer induce canonical signaling

To investigate Reelin signaling in neurons, we established primary cultures dissociated from embryonic day 16 mouse cerebral cortices and kept them *in vitro* for 4–10 days (DIV4–10). We first characterized DIV4 cultures using an IN Cell analyzer (Cytiva) for high-content analysis (HCA) of fluorescence microscopy images, which enabled us to analyze thousands of cells in an unbiased manner, thus establishing a high-throughput assay for signal transduction experiments. All neurons were detected by immunofluorescence using four antibody markers (MAP2, TUJ1, HuCD, and NeuN), GABAergic neurons were specifically detected using the anti-GAD67 antibody, and astrocytes were detected using an anti-GFAP antibody (Table S1). The cultures were then counterstained with Hoechst stain to identify all cell nuclei (Figure S2A). Randomized fluorescence images revealed that most cells in culture were neurons, with extensive dendrites (visualized by MAP2) and axons (TUJ1). The nuclei of all neurons were clearly detected by the pan-neuronal nuclear marker HuCD, and the nuclei of mature neurons were detected by NeuN staining. GAD67$^+$ inhibitory neurons were also readily identified, and very few GFAP$^+$ astrocytes were present. These data indicated that neurons (HuCD$^+$ cells) represented approximately 70% of all the cells in culture, whereas approximately 50% of all cells were mature neurons (NeuN$^+$) and 20% were GABAergic (GAD67$^+$) interneurons (Figure S2B). Taken together, these data suggest that ~50% of all cells in culture were excitatory neurons, ~20% were inhibitory neurons, and 30% were glia, fibroblasts, undifferentiated precursors, or unhealthy, dying cells.

We used the HCA imaging methodology to investigate the activation of the canonical signaling pathway by FL and cleaved Reelin fragments in DIV4 mouse cortical cultures. As a positive control we used 10% fetal bovine serum (FBS), and as a negative control we used the Reelin purification buffer. Cultures were stained with Alexa 488-conjugated antibodies directed against phosphorylated ribosomal protein S6 (pS6), a well-known target of the PI3K/Akt/mTOR pathway, and thus a downstream readout of the Reelin canonical pathway (Ballif et al., 2003). Cells were double labeled with HuCD primary antibodies and CY5-conjugated secondary antibodies, to identify neuronal cells, and counterstained with Hoechst to detect all nuclei. As expected, a clear pS6 signal was detected in the cytoplasm of many cells, whereas a strong HuCD stain was detected in most nuclei, overlapping with the Hoechst stain (Figure 2A). The percentage of pS6$^+$ cells under each treatment condition was determined from the analysis of several thousand cells in triplicate sample wells. The data show that only Reelin FL and the dimeric CF-Fc (both at 50 nM concentration) induced a significant increase in the percentage of pS6$^+$ cells identified by Hoechst stain (Figure 2B). The monomeric CF C2101A, like other proteolytic products, did not induce S6 phosphorylation at the same concentration. We also analyzed the percentage of pS6$^+$ neurons (HuCD$^+$) (Figure 2C) and the intensity of the pS6 signal in all cells (Figure 2D), and again observed that only Reelin FL and dimeric CF-Fc induce pS6. The data imply that only Reelin FL and the dimeric CF can interact with lipoprotein receptors, VLDLR/ApoER2, and activate canonical signaling. The statistically significant induction of pS6 by Reelin FL and CF-Fc was replicated in additional HCA experiments using independent cortical cultures (data not shown).

To confirm the HCA immunofluorescence findings using traditional biochemical techniques, we exposed cortical cultures to purified Reelin proteins as above and performed western blot analysis of Akt phosphorylation using anti-phospho-Akt Ser473 (pAktS)- and anti-phospho-Thr308 (pAktT)-specific antibodies. To normalize the data for protein content, the blots were reprobed with antibodies against total Akt. The ratio of pAkt/total Akt was calculated and plotted from two independent experiments (Figure S3). Even though these experiments were not sufficient to conduct a statistical analysis, the results support the observed pattern in Figure 2, as only Reelin FL and CF-Fc induce Akt phosphorylation (and thus canonical signaling), whereas other Reelin fragments, including the monomeric CF C2101A, are ineffective.

The expression of IEGs *Arc* and *c-Fos* was used as a readout of the non-canonical signaling downstream of Erk1/2 activation.

Please cite this article in press as: Turk et al., The structure-function relationship of a signaling-competent, dimeric Reelin fragment, Structure (2021), https://doi.org/10.1016/j.str.2021.05.012

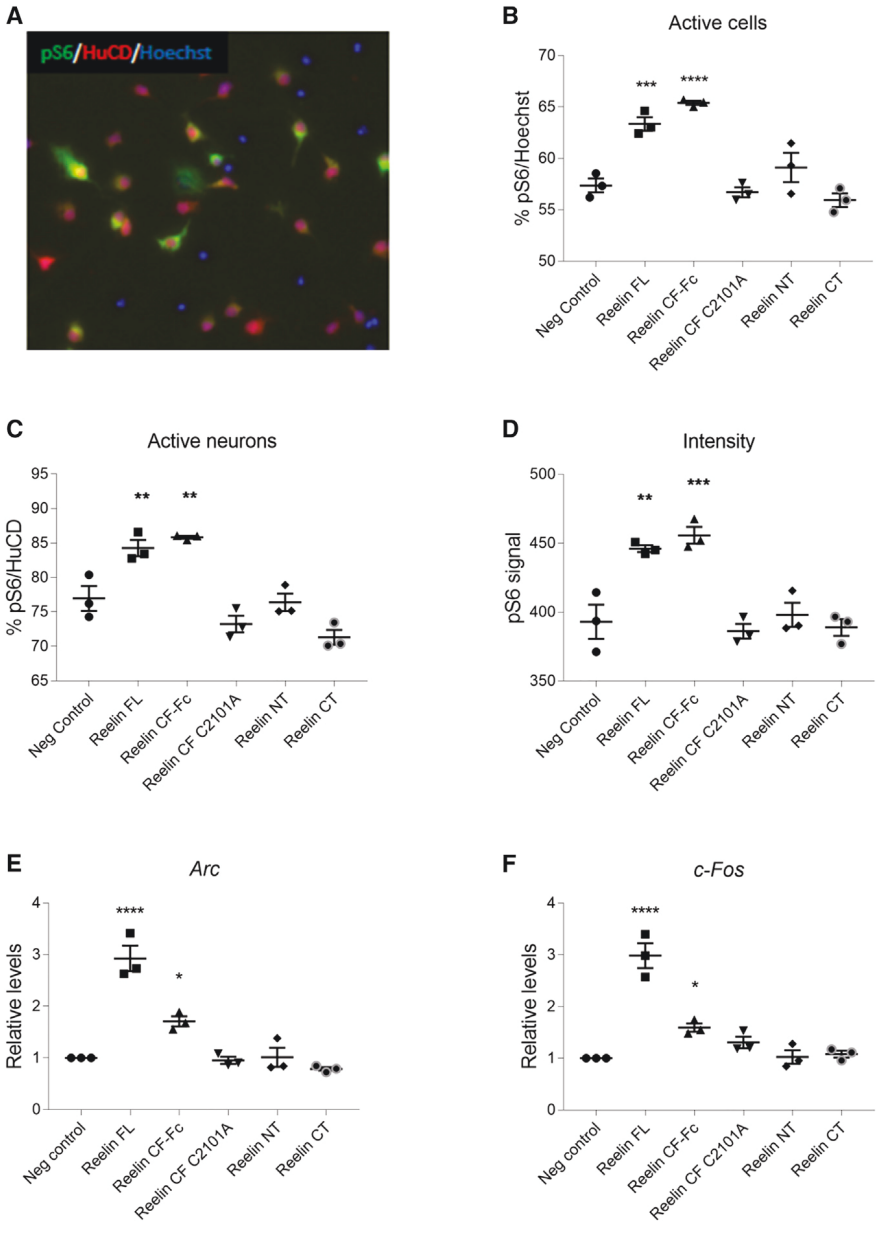

Figure 2. Induction of canonical and non-canonical signaling pathways by Reelin fragments

Neurons were treated with various purified Reelin fragments at 50 nM, and readouts of canonical and non-canonical signaling pathways were assessed using HCA of fluorescence images and qRT-PCR, respectively.

(A) Representative image of HCA immunofluorescence experiment. Green, pS6; red, HuCD; blue, Hoechst.

(B–D) Statistical analysis of the percentage of $pS6^+$ neurons in all cells (B) and in neurons (C), and the overall intensity of pS6 signal (D) in DIV4 neurons.

(E and F) Quantification of relative levels of *Arc* (E) and *c-Fos* (F) as measured by qRT-PCR in DIV10 neurons. One biological experiment of three technical replicates was used to generate the figure. Each data point corresponds to a single well, which is an average of nine individual fields of view. Each technical replicate (well) comprised >1,000 cells.

$^*p \leq 0.05$; $^{**}p \leq 0.01$; $^{***}p \leq 0.001$; $^{****}p \leq 0.0001$.

We exposed cortical cultures to purified Reelin proteins, extracted total RNA, and analyzed *Arc* and *c-Fos* expression by qRT-PCR. Values were normalized to the ribosomal protein *S12* gene as an internal control. The data from three independent experiments demonstrate that Reelin FL strongly induced both *Arc* and *c-Fos* expression, whereas CF-Fc caused a small induction; other Reelin fragments had no effect (Figures 2E and 2F). Consistent with previous reports, these results show that only Reelin FL is capable of inducing a robust activation of non-canonical signaling (Lee et al., 2014).

Dimeric Reelin CF binds to the ectodomains of ApoER2 and VLDLR with a higher affinity than its monomeric form

To begin examining why the dimeric CF elicits canonical signaling but the monomeric CF does not, we used bio-layer interferometry (BLI) to measure binding affinities between Reelin constructs of different oligomeric states and the receptors involved in the canonical signaling pathway (ApoER2 and VLDLR). Fc-fused receptor ectodomains (Figure S4) were immobilized to protein A biosensors (ForteBio); using a dilution series of purified Reelin proteins, we calculated the dissociation constant (K_D) between each receptor and the following Reelin constructs that contain the lipoprotein-receptor-binding central domain: Reelin FL, dimeric Reelin CF, monomeric Reelin CF, and mutant monomeric Reelin CF C2101A (Figures 3 and 4). Dimeric and monomeric CF proteins used in these assays were separated from each other by SEC and did not contain the Fc. Consistent with previous reports (Yasui et al., 2010, 2011), we found that all Reelin proteins bound more tightly to ApoER2 compared with VLDLR; affinities of Reelin proteins for ApoER2 ranged from 57 to 477 nM, whereas for VLDLR, affinities ranged from 200 to 8,440 nM (Table 1). However, the binding affinities of different Reelin proteins for each receptor followed a similar pattern, with Reelin FL exhibiting the tightest binding, followed by the CF dimer, and then the two monomeric forms. Reelin binding is dependent on the receptors' coordination of calcium ions near the binding site; therefore we included EDTA in the dissociation buffer of the BLI experiments to disrupt binding and return the signal to baseline. Since we calculated the K_D by fitting the maximum signal at each concentration using a non-linear regression, the inclusion of 1 mM EDTA in the dissociation step had no impact on the analysis but allowed the sensor to be reused at other protein concentrations. Interestingly, even when using EDTA during the dissociation between ApoER2 and both Reelin FL and CF dimer, we were unable to

Please cite this article in press as: Turk et al., The structure-function relationship of a signaling-competent, dimeric Reelin fragment, Structure (2021), https://doi.org/10.1016/j.str.2021.05.012

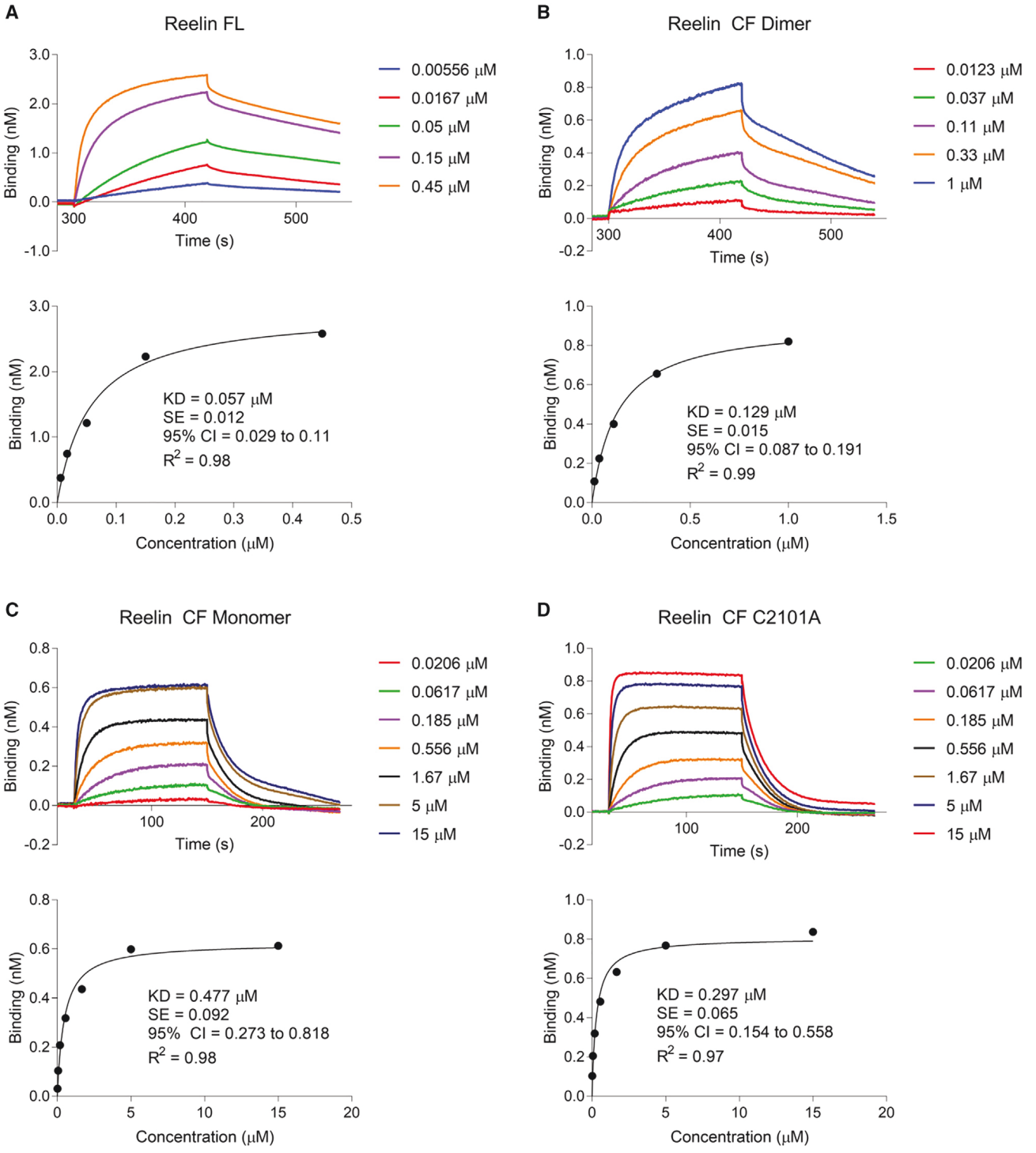

Figure 3. Binding curves detailing the interaction between ApoER2 and Reelin fragments

BLI protein A sensor tips were loaded with ecto-ApoER2-Fc and exposed to a dilution series of purified Reelin constructs to calculate the interaction affinities. (A–D) (Top) Individual binding curves of purified Reelin constructs at various concentrations (right) featuring characteristic phases of association (120 s) and dissociation (120 s). (A) Reelin FL, (B) Reelin CF dimer, (C) Reelin CF monomer, (D) Reelin CF C2101A. (Bottom) Maximum responses at the measured concentrations were plotted and fitted with a one-site-specific, non-linear regression to calculate a K_D for each interaction (GraphPad Prism8). SE, standard error; CI, confidence interval. The BLI curves in (A) and (B) are single measurements, while those in (C) and (D) are averages of two measurements at each concentration.

Please cite this article in press as: Turk et al., The structure-function relationship of a signaling-competent, dimeric Reelin fragment, Structure (2021), https://doi.org/10.1016/j.str.2021.05.012

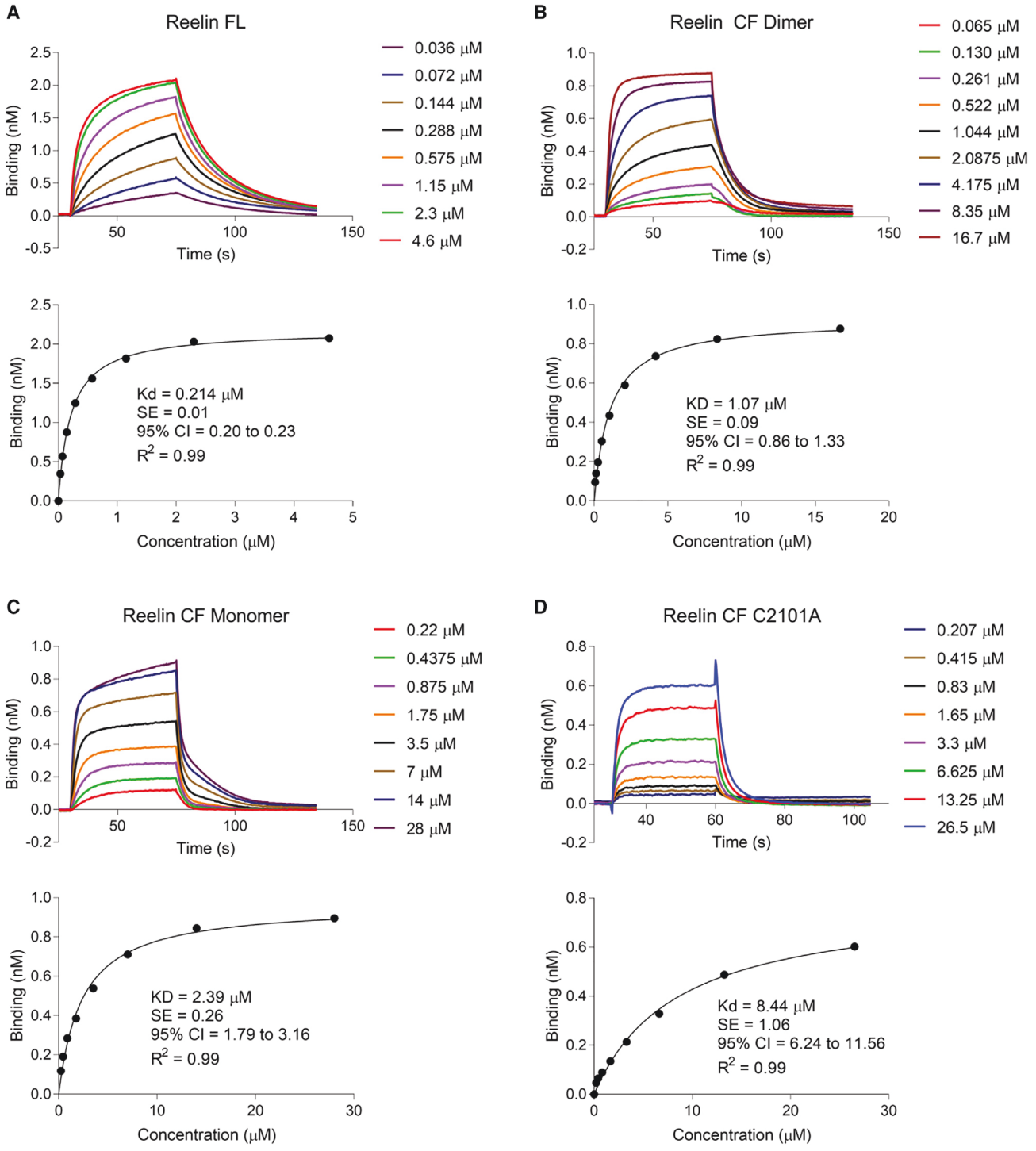

Figure 4. Binding curves detailing the interaction between VLDLR and Reelin fragments

Similar to BLI data presented in Figure 3, K_D was calculated using a dilution series of the same Reelin fragments but this time loading the BLI biosensors with ecto-VLDLR-Fc.

(A–D) (Top) Individual binding curves of purified Reelin constructs at various concentrations. (A) Reelin FL, (B) Reelin CF dimer, (C) Reelin CF monomer, (D) Reelin CF C2101A. (Bottom) Maximum responses at the measured concentrations were again plotted and fitted to calculate a K_D for each interaction. SE, standard error; CI, confidence interval. BLI curves are an average of either two individual measurements (A) or three individual measurements (B–D).

observe a complete dissociation, leading us to use a fresh protein A biosensor for each concentration measured (Figure S4). We then compared the dissociation phases between each Reelin construct and both receptors in the presence or absence of calcium (Figure S5). Particularly apparent in the ApoER2 binding dataset is the complete lack of dissociation of FL and CF dimeric

Please cite this article in press as: Turk et al., The structure-function relationship of a signaling-competent, dimeric Reelin fragment, Structure (2021), https://doi.org/10.1016/j.str.2021.05.012

Table 1. BLI calculated binding affinities

BLI calculated dissociation constants (μM)		
Reelin protein	ApoER2	VLDLR
Reelin FL	0.057 (0.029–0.11)	0.21 (0.20–0.23)
Reelin CF dimer	0.129 (0.087–0.191)	1.07 (0.86–1.33)
Reelin CF monomer	0.477 (0.273–0.818)	2.39 (1.79–3.16)
Reelin CF C2101A	0.297 (0.154–0.588)	8.44 (6.24–11.56)

K_D values as calculated from the measurements presented in Figures 3 and 4. The K_D 95% confidence interval is in parentheses.

proteins in the presence of calcium compared with the monomeric CF proteins that dissociate from the receptor in the presence of calcium, albeit more slowly than when calcium is excluded from the system. This pattern is also observed in the VLDLR dataset, with Reelin FL not dissociating from the receptor, while the monomeric CF proteins readily dissociate in the presence of calcium, especially the CF C2101A protein. The CF dimer does gradually dissociate from VLDLR in the presence of calcium, which is not unexpected given the relatively weaker K_D of the interaction (1.07 μM) compared with the K_D of the interaction between this Reelin protein and ApoER2 (129 nM). Overall, the binding data demonstrate that Reelin proteins have higher affinities for ApoER2 compared with VLDLR; they also highlight the receptors' higher affinities for the dimeric CF compared with the monomeric proteins. The differential affinities are, in part, likely a result of the comparatively low rate of dissociation between receptors and the FL or the dimeric CF Reelin ligands, as they form complexes that are tightly held together in the presence of calcium.

Monomeric Reelin CF C2101A does not signal even at a high concentration

Having measured weaker binding affinities between ApoER2 or VLDLR and CF C2101A compared with the dimeric proteins, we considered the possibility that the monomeric protein might have failed to elicit signaling in our previous HCA experiment (Figures 2A–2D) due to the relatively low concentration used in the assay (50 nM). In BLI experiments, the K_D for the interactions between CF C2101A and lipoprotein receptors was 0.297 and 8.44 μM (ApoER2 and VLDLR, respectively; Figures 3D and 4D). Therefore, we repeated the HCA experiment, treating the dissociated neurons with CF C2101A at 10 μM to ensure a sufficient Reelin concentration in the assay. Treatment with 10 μM CF C2101A (200-fold higher than the concentration of the CF dimer that induced canonical signaling) still failed to cause a significant increase in pS6 compared with the negative control (Figure 5), suggesting that this protein is truly signaling incompetent. Thus, the observed lack of signaling activity is not due solely to the comparatively lower binding affinity of monomeric CF C2101A, but likely reflects the inability of this ligand to alter the conformation of lipoprotein receptors in a way that initiates signal transduction.

Cryo-ET of Reelin CF

To understand the structural basis for the differential activities and binding capacities of monomeric and dimeric Reelin CF, we used cryo-ET to resolve their 3D structures.

The monomeric CF was easily identified as elongated fragments with each RR resolved as a globular density about 40 Å in width and 60 Å in length. The CF monomers display high levels of structural heterogeneity in overall shape and curvature (Figure 6A). The four repeats in the CF monomer (RR3–RR6) vary in their arrangement, from aligning themselves in a relatively straight line to bending as an arch at variable degrees. Subtomogram analysis and averaging algorithms failed to generate converged class averages for the monomers, even when a large class number was used, suggesting that the conformational flexibility of the monomers is probably continuous in solution.

In tomograms of CF dimers, the two protein chains appear to be more rigid compared with the CF monomer, and they intersect one another to form an X shape (Figure 6B). Initial model-free classification of 7,729 CF dimer subtomograms generated eight unique class averages, all displaying apparent C2 symmetry. Thus, C2 symmetry was applied to all subsequent subtomogram alignment and averaging steps in our analysis. Structural analysis of the subtomogram averages revealed a high level of heterogeneity in the angle between the two protein chains and flexibility in the position of the repeats on either end of the fragment (RR3 and RR6). To achieve a more homogeneous population for structural analysis, we proceeded with a second iteration of subtomogram classification and averaging, including only CF dimer subtomograms with all four repeats in both protein chains clearly resolved (Figure 6C).

Subtomogram analysis and classification on the selected subset of particles (n = 1,708) resolved the dimerization site between the two protomers, as expected, on RR5. Using this dimerization site as a landmark, we measured the angle between the vectors formed by the four repeats in the two protomers (Figure S6A). In this subset, the two protein chains cross each other in a parallel configuration at an angular range of 43°–71° (Figures 6D and Table S2). The distances between the two intersecting chains, defined as the distance between the C-terminal ends of RR6 on each protomer (Figure S6A), range from 71 to 86 Å (Figure 6D, Table S2). In all subtomogram averages, despite the different crossing angles and distances, the two protomers share an extended conformation, with all four repeats generally aligning along a straight line.

After combining particles from classes with similar crossing angles (classes 1, 2, 3, and 8 in Figure 6D) and further refining particle alignment, we generated a 3D average of the CF dimer at ~20 Å resolution (Figure 6E). At this resolution, each protein chain can be confidently segmented into four subunits, corresponding to the four repeats, RR3–RR6 (Figure 6E). The two subrepeats within each Reelin repeat are also delineated. The dimerization site is identified on subrepeat A of RR5. Fitting models of individually solved crystal structures of Reelin repeats into the subtomogram average reveals that C2101, the residue responsible for the dimeric structure of Reelin, unequivocally aligns within the dimerization site in the density map (Figures S6B and S6C). This conformation allows for both receptor-binding sites (K2360/K2467), one on each monomer, to remain exposed on opposite sides of the dimerization interface (Figure S6D).

Solution scattering of Reelin CF monomer

To use an independent, in-solution, structural technique, we fractionated the sample and collected SAXS data of monomeric Reelin CF (Figure S7A, Tables S3 and S4). The excellent quality of the protein preparation was apparent by the linearity of the Guinier plot, indicative of a monodisperse sample with no

Please cite this article in press as: Turk et al., The structure-function relationship of a signaling-competent, dimeric Reelin fragment, Structure (2021), https://doi.org/10.1016/j.str.2021.05.012

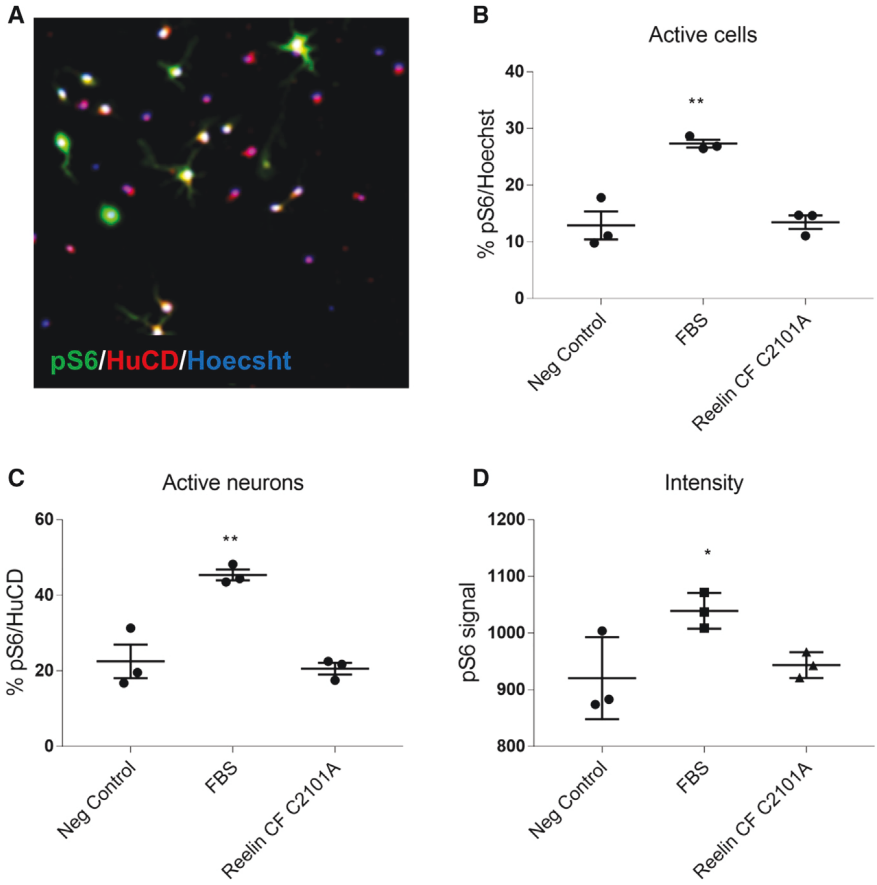

Figure 5. Treatment with a high concentration of Reelin CF C2101A does not induce pS6 in dissociated neurons

DIV4 mouse neurons were treated with 10 μM Reelin CF C2101A to ensure a sufficient concentration of monomeric Reelin to interact with the canonical pathway receptors based on the BLI calculated K_D (see Figures 3 and 4).

(A) Representative image showing pS6 (green), HuCD (red), and Hoechst (blue) staining.

(B–D) Treatment with 10 μM CF C2101A does not activate canonical pathway signaling in all cells (B) or neurons (C) or as a measure of intensity (D). Ten percent FBS was included as a positive control; the protein purification buffer was included as a negative control. One biological experiment of three technical replicates was used to generate the figure. Each data point corresponds to a single well, which is an average of nine individual fields of view. Each technical replicate (well) comprised >1,000 cells.

*$p < 0.05$; **$p < 0.01$.

detectable aggregation (Figure S7B). The radius of gyration for the CF monomer (66.54 Å) is consistent with the observations made using cryo-ET that the protein adopts an elongated conformation. We performed a P(r) analysis to provide information regarding the maximum linear dimension (D_{max}) of the particle in solution. The P(r) curve smoothly approaches the x axis when the D_{max} is set to 245 Å (Figure S7C), supporting the concept that the monomeric Reelin CF is an extended molecule with each subunit contributing ~60 Å in length. The dimensionless Kratky plot is bell shaped, indicative of a folded protein (Figure S7D). The observed molecular weight through Bayesian inference of the monomeric CF is 185.8 kDa (Table S5). Compared with the expected MW of 190.8 kDa, with nine putative N-linked glycosylation sites (based on primary structure) taken into account, the observed MW and expected MW differ by only ~2.6%.

Since the preliminary parameters indicate that the sample preparation is of good quality, we used DAMMIN *ab initio* bead modeling to determine a low-resolution, 3D structure of the SAXS data. Averaging and filtering the bead models, using DAMAVER and DAMFILT, yields models portraying the protein consistently as an extended rod with visible domains, a maximum length of ~240 Å, and a cross-sectional diameter of ~45 Å (Figure S7E, Table S6). The rigid-body modeling software SASREF fits four Reelin repeat models to the SAXS data with a χ^2 of 1.48 and builds a model using individual domains (previously determined by X-ray crystallography or homology) that resembles the cryo-ET structure (Figures S7F and S7G, Table S7). Two SAXS bead models were aligned in the cryo-ET volume map of dimeric Reelin CF, using Chimera's Fit in Map module, and they fit the data well (Figure S7H). Although SAXS reconstructions for the CF monomer were virtually identical to the individual protomers within the cryo-ET solution, SAXS did not reliably resolve the CF dimer structure due to higher order particles in the purified preparation (data not shown). We attribute this to a not-yet-optimized purification procedure, which was later resolved and utilized in other experiments (e.g., BLI, AUC). We did not reattempt to gather SAXS data of the dimer after having optimized the purification, since we had already resolved the dimer via cryo-ET, which is a higher resolution technique and also provides an in-solution structure.

Analytical ultracentrifugation

To analyze the hydrodynamic behavior of Reelin CF, we conducted SEC and sedimentation velocity AUC experiments (Figure 7). Together, they demonstrate a lack of concentration-dependent self-association among the different oligomeric states of Reelin CF (Figure 7A). Although the SEC and AUC data for Reelin CF present multiple species, the sedimentation velocity profiles at concentrations of 0.057, 0.18, and 0.4 g/L reveal that the relative proportions of the sedimented solutes remain constant, supporting the concept that the oligomerization state of Reelin CF is not dependent on concentration.

To limit overlapping signals during the AUC runs and to calculate precise hydrodynamic parameters for each of the solutes present in the purified preparation of Reelin CF, we prepared AUC samples after two consecutive SEC fractionation runs. During the first run, we collected fractions corresponding to the main peaks in the SEC profile (Figure 7A) and ran these fractions though the SEC column a second time to ensure separation of the different-sized solutes. The AUC data from these different

Please cite this article in press as: Turk et al., The structure-function relationship of a signaling-competent, dimeric Reelin fragment, Structure (2021), https://doi.org/10.1016/j.str.2021.05.012

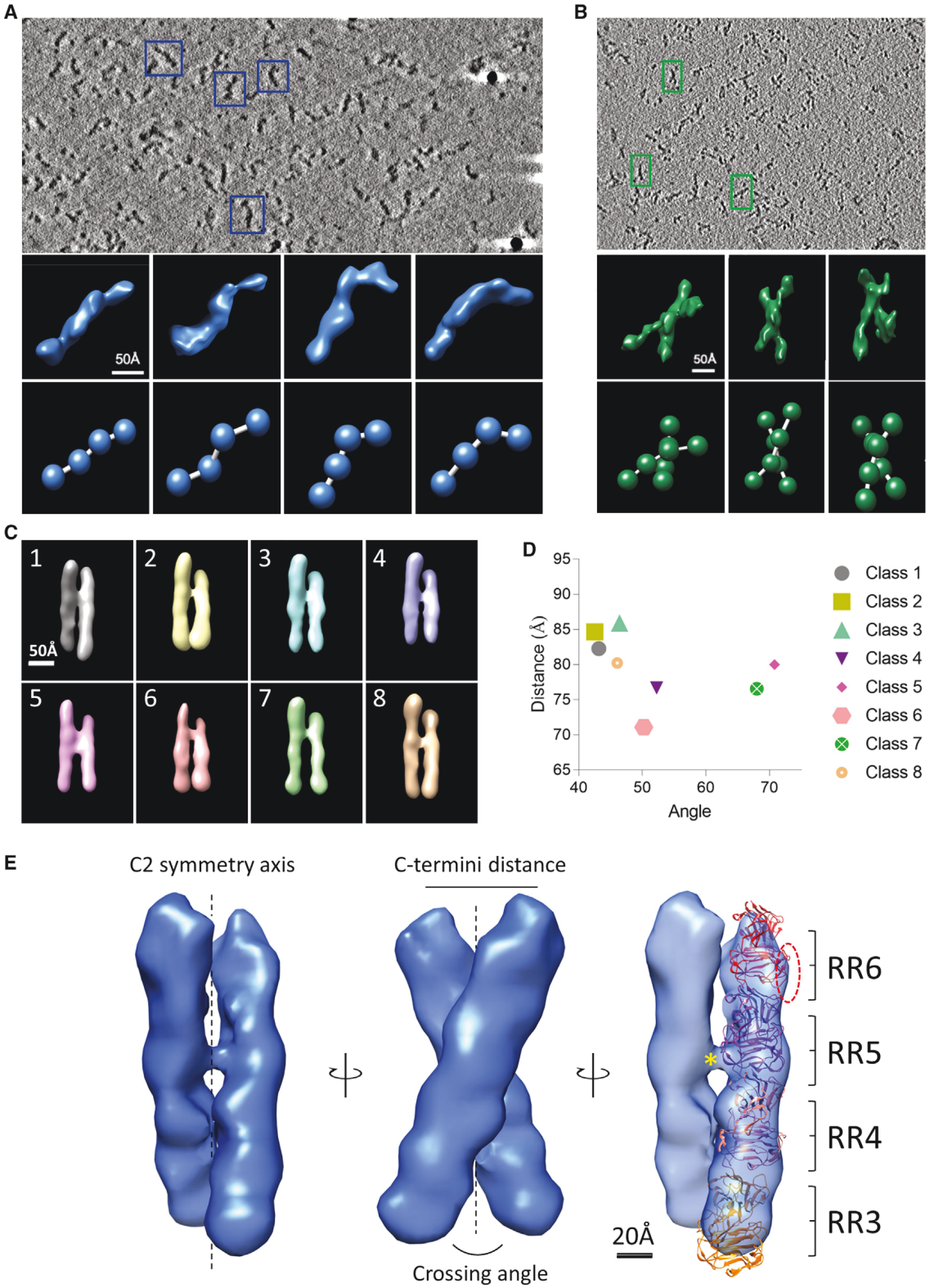

Figure 6. Structure of Reelin CF by cryo-ET

(A) Slice view of a tomogram of fractionated Reelin CF monomers and isosurface views of representative CF monomer subtomograms (blue boxes). The 3D models of the subtomograms (bottom) are shown to reveal the relative spatial relationship of the four repeats (RR3–RR6).

(B) Slice view of a tomogram of fractionated Reelin CF dimers and isosurface views of representative CF dimer subtomograms (green boxes).

(C) Classification and averaging of Reelin CF dimers revealed structural and/or compositional heterogeneity.

(legend continued on next page)

Please cite this article in press as: Turk et al., The structure-function relationship of a signaling-competent, dimeric Reelin fragment, Structure (2021), https://doi.org/10.1016/j.str.2021.05.012

fractions (Figures 7B–7D) are consistent with all the structural data presented in the paper (Table S8). Interestingly, the higher-order peak (9.5–12.5 mL in the SEC) does not resolve as a single species, but rather as a collection of solutes (8–30 S) that cannot easily be assigned an oligomeric state (Figure 7B), likely representing biologically irrelevant, soluble aggregates. However, the peak at 10.7 S (12.5–13.5 mL in the SEC) is clearly resolved and has an apparent MW of 332 kDa and a frictional ratio (f/f0) of 1.65 (Figure 7C), consistent with an elongated dimeric protein that is observed in the cryo-ET data. Similarly, the SEC fraction from 13.5 to 15 mL is also well resolved (~7 S) and has an apparent MW of 174 kDa and f/f0 of 1.62 (Figure 7D), consistent with an elongated monomer, as seen in the SAXS and cryo-ET data. Reelin CF C2101A is also a single species of ~174 kDa with an f/f0 of ~1.66 (Figure S8).

A heterodimeric Reelin fragment induces canonical pathway signaling in dissociated neurons

So far, we have confirmed that both the Reelin CF dimer and the monomer bind to ApoER2 and VLDLR, but only the CF dimer can elicit canonical pathway signaling. To further investigate the apparent decoupling of binding and signaling, we utilized a heterodimeric (HD) Reelin construct. Following our established protocol (Turk et al., 2020), we used tandem affinity chromatography to purify a Reelin CF HD protein composed of both a wild-type chain and another chain carrying a mutation that abolishes the receptor-binding site (K2467A) (Figure S9). As such, Reelin CF HD should be able to bind to only a single receptor molecule. Performing another HCA experiment, we treated dissociated mouse cortical neurons with Reelin CF HD at concentrations of 200 and 50 nM (Figures 8 and S10, respectively). After treatment with either concentration of HD protein, we detected a strong induction of canonical signaling similar to that elicited by the wild-type homodimer, as measured by the fraction of $pS6^{+}$ cells or neurons and signal intensity. This finding supports a model where dimeric Reelin alone has the necessary conformation to engage a single lipoprotein receptor in a manner that leads to signaling events. The HCA experiment was repeated using 200 nM HD protein to treat an independent culture, and the results were reproduced (data not shown).

DISCUSSION

Although several studies have characterized many of the Reelin's biological functions in the brain and the underlying molecular mechanisms (for recent reviews see Bock and May, 2016; Hirota and Nakajima, 2017; Lee and D'Arcangelo, 2016; Lussier et al., 2016; Ranaivoson et al., 2016; Wasser and Herz, 2017), detailed structural information of a signaling-competent ligand has yet to emerge. The paucity of structures is likely due to the large size of Reelin, its inherent flexibility, and the fact that the secreted protein is subject to a complex pattern of proteolytic cleavage *in vivo* and *in vitro*.

To better understand the relationship between Reelin protein structure and function, we used a combination of high-throughput imaging analysis of signal transduction events in cultured neurons, as well as advanced biophysical and biochemical techniques. Here we showed that: (1) as expected, the purified dimeric CF is sufficient to activate the canonical Reelin signaling pathway leading to S6 phosphorylation, whereas the purified monomeric CF, even at 200-fold higher concentrations, does not induce measurable signal transduction. The present data also confirmed our previous observation that only the FL Reelin protein robustly activates the non-canonical pathway leading to IEG expression (Lee et al., 2014). (2) The dimeric Reelin CF binds to its receptors, ApoER2 and VLDLR, with affinities that are only 2- to 8-fold higher than those of the monomeric fragment. These data suggest that the lack of signal activation by the monomeric fragment is not simply due to reduced affinity, but rather that signaling requires a ligand conformation that is specific to the dimeric protein. (3) The 3D structure obtained by cryo-ET and subtomogram analysis reveals the architecture of the dimeric form of Reelin CF. We complement this structure and confirm the structure of the monomeric form, previously reported by other groups (Nogi et al., 2006), using SAXS and AUC.

One of our main findings is that the signaling-competent Reelin CF is a covalent parallel dimer. While each protomer appears relatively rigid, with the individual repeats aligned nearly on a straight line (Nogi et al., 2006), RR3 and RR6 display some flexibility to the extent that three-quarters of the initial class averages displayed relatively poorer definition in these regions compared with the two central domains (RR4 and RR5). Intermolecular flexibility of the two protomers relative to each other is also present, as measured by the torsional angle between protomers and the distance between markers placed at the C-terminal ends of RR6 on each protomer. The dimeric CF assumes an X shape that enables the receptor-binding sites of each RR6 to remain available, enabling Reelin to bind to the lipoprotein receptors in a conformation that can stimulate canonical signaling through both ApoER2 and VLDLR. The observed stability of the central domains (RR4 and RR5) and flexibility of the outer two domains (RR3 and RR6), along with the visible overlap of RR4 and RR5, lead us to speculate that there may be a shared interface between RR4 and RR5 on each protein chain that adds to the overall dimeric stability. The overlapping RR4 and RR5 domains may provide a source of stability through non-covalent protein-protein interactions maintaining the dimer's X-like conformation, so that it does not freely rotate about the disulfide bond at C2101. The dichotomous properties of flexibility and stability made the CF dimer a prime candidate for analysis using cryo-ET. Cryo-ET was well suited to this application because the heterogeneity of the dimer did not allow us to confidently average large datasets to be used in single-particle cryo-EM, while still being able to generate class averages and refine a model to ~20 Å resolution (Dai et al., 2013; Turk and Baumeister, 2020).While not as detailed, these results were supported and

(D) Markers of structural heterogeneity within the CF dimer classes (see [E], Figure S6A, and Table S2 for details).
(E) Subtomogram average of predominant classes of Reelin CF dimers clearly revealed the dimerization site and C2 symmetry. The side and the tilted views of the final subtomogram average map of CF dimers demonstrate the approximate parameters used for measuring structural heterogeneity (see Figure S6A for a more detailed schematic). Fitting of high-resolution RR5–RR6 X-ray crystallography structures (PDB: 2E26) aids in the demarcation of Reelin repeat boundaries. Yellow asterisk denotes the position of C2101 on the monomer. Dashed ellipse: receptor-binding site.

Please cite this article in press as: Turk et al., The structure-function relationship of a signaling-competent, dimeric Reelin fragment, Structure (2021), https://doi.org/10.1016/j.str.2021.05.012

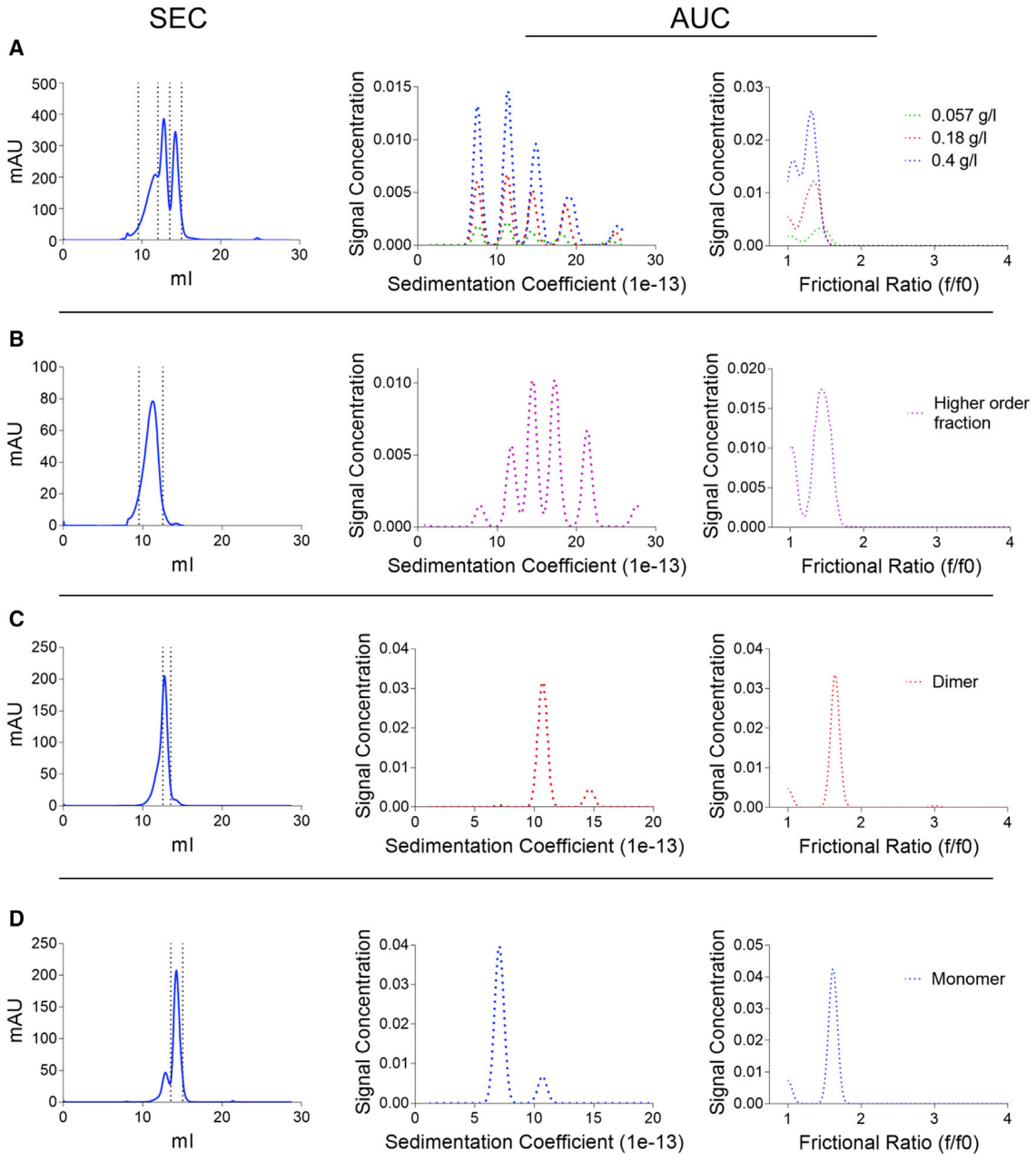

Figure 7. Analytical ultracentrifugation of Reelin CF

SEC curves (left) and the corresponding AUC data outlining the hydrodynamic properties of Reelin CF are shown.

(A) Three different concentrations of unfractionated Reelin were used to detect or rule out concentration-dependent oligomerization. Fractionation boundaries used for (B–D) are shown (left).

(B) The higher-order fraction is made of several species, likely representing biologically irrelevant aggregates.

(C) Fractionated dimeric Reelin CF sediments primarily as a single species (86.4%) of 10.7 S (~332 kDa) with a frictional ratio of 1.65.

(D) Fractionated monomeric Reelin CF sediments primarily as a single species (85.2%) of 7.1 S (~174 kDa) with a frictional ratio of 1.62.

strengthened by the independent in-solution techniques of SAXS, SEC, and AUC, generating high-confidence datasets. Interestingly, SEC and AUC enabled us to identify aggregation within the Reelin CF sample preparation and rule out the presence of a biologically relevant tetramer. These high-molecular-weight multimers that appear during the purification of the CF dimer do not display any concentration-dependent self-association, nor are they likely physiologically relevant, but rather they are probably artifactual aggregates. Taken together, these data provide information on the oligomerization, architecture, and orientation of the CF in a signaling-competent construct.

The Reelin-receptor-binding experiments highlight the greater affinity that Reelin has for ApoER2 relative to VLDLR, regardless of oligomeric state, and also the greater affinity that both

Please cite this article in press as: Turk et al., The structure-function relationship of a signaling-competent, dimeric Reelin fragment, Structure (2021), https://doi.org/10.1016/j.str.2021.05.012

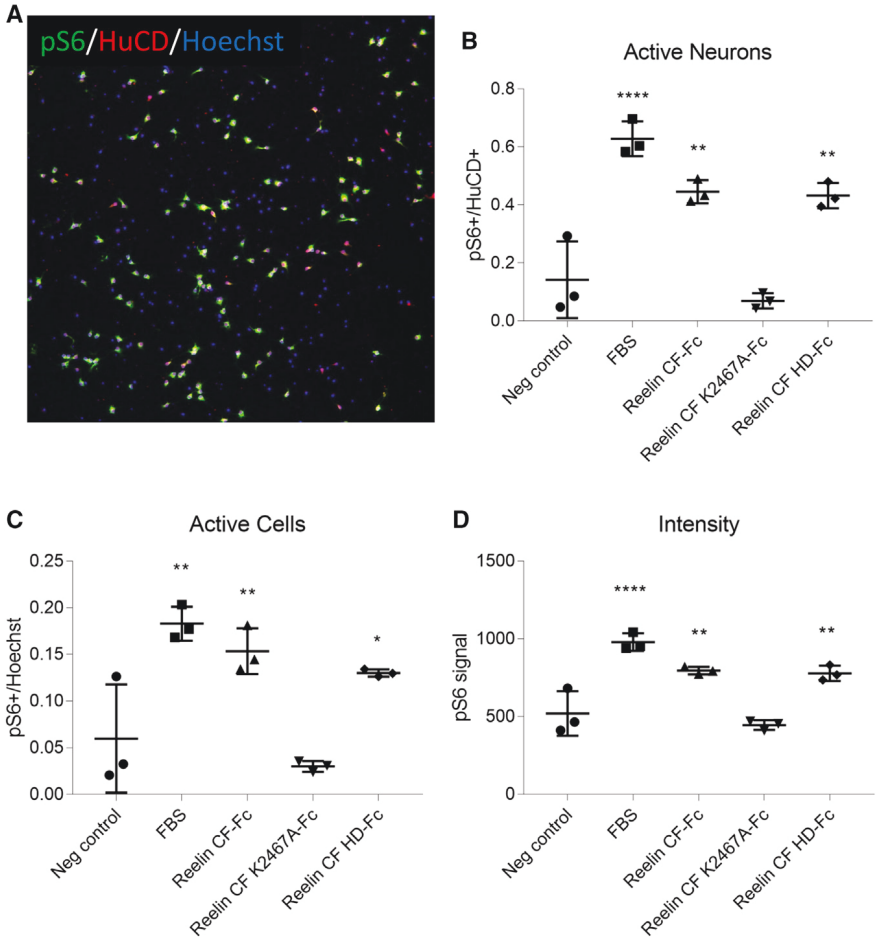

Figure 8. Heterodimeric Reelin fragment activates canonical signaling pathway in dissociated neurons

DIV5 primary mouse cortical neurons were treated with 200 nM purified Reelin proteins, and activation of the canonical signaling pathway was measured using HCA imaging.

(A) Representative image of HCA immunofluorescence experiment; green, pS6; red, HuCD; blue, Hoechst.

(B–D) Induction of S6 phosphorylation was measured as the percentages of $pS6^+$ neurons ($HuCD^+$) (B) and $pS6^+$ cells (Hoechst) (C) as well as the overall pS6 intensity (D). This figure is representative of a single biological experiment. Each data point corresponds to a single well, which is an average of nine individual fields of view. Each technical replicate (well) contains >1,000 cells.

*p ≤ 0.05; **p ≤ 0.01; ****p ≤ 0.0001.

receptors have for dimeric forms of Reelin compared with monomeric forms. Furthermore, we observed a particularly slower dissociation phase in the BLI experiments for dimeric constructs, likely a contributing factor in the comparatively tighter dimeric K_D. Analysis of the available structure of ecto-ApoER2 and RR5–RR6 (Yasui et al., 2010) reveals the interface that occurs between ligand and receptor, and its dependence on the caging of a Ca^{2+} ion by a number of Glu and Asp residues that in turn interact with Lys at residues 2,467 and 2,360 on Reelin. However, comparing the primary structure between ApoER2 and VLDLR at the receptor-binding site provides no clearly observable reason as to the lower affinities measured (e.g., lack of acidic residues) between Reelin constructs and VLDLR. We therefore hypothesize that broad, gradual differences in the tertiary structures of ApoER2 and VLDLR affect the interaction between them and Reelin constructs, sterically favoring the interaction between ApoER2 and Reelin. However, a structure of the Reelin dimer and VLDLR complex would be necessary to adequately address this hypothesis.

Fitting the dimeric CF's cryo-ET volume map with high-resolution structures of previously solved RRs (Yasui et al., 2007; PDB: 2E26) directly reveals that the receptor-binding site on each protein chain is solvent accessible. This suggests that the dimeric CF may bind to two receptors simultaneously, and this may be a potential mechanism of signal activation. As we show in this study, the fact that the CF dimer initiates signal activation, while the CF monomer does not, is likely a result of the dimeric ligand's conformation and not a product of the monomer's lower binding affinity. Two potential mechanisms may explain the dimer's unique signaling capability: (1) the dimeric ligand binds to two receptors simultaneously, causing an increased local concentration of receptors in an active conformation that is required for signal transduction, or (2) the dimeric protein does not bind to two receptors, but rather adopts an X-like conformation that allows it to interact with lipoprotein receptors and produce an active ligand-receptor complex that cannot be formed by the monomeric ligand. To distinguish between these possibilities, we generated a Reelin CF heterodimer that has a single receptor-binding site and tested its ability to induce canonical pathway activation. The finding that heterodimer treatment caused strong signaling supports the mechanism in which Reelin dimers alone can activate the VLDLR/ApoER2-mediated signaling pathway by binding to a receptor and forming a unique dimer-receptor complex that is necessary to initiate the intracellular signal cascade. Our results are complementary to those of a previous study in which Reelin was shown to induce clustering between FL ApoER2 and an ApoER2 construct with its ligand binding site deleted (Divekar et al., 2014). Receptor clustering has been shown to be involved in initiating Reelin's canonical signaling pathway (Divekar et al., 2014; Strasser et al., 2004). Viewed in conjunction with these previous observations, our data suggest a model in which each Reelin dimer has a conformation that enables it to bind to a single receptor molecule and alter its conformation, thus creating a clustering-prone ligand-receptor complex that serves as a hub for canonical signaling pathway activation (Figure 9).

A future direction that may be useful to further dissect the molecular mechanism of signal activation by Reelin would be to investigate the signaling properties of HD deletion constructs. Our model suggests that Reelin's secondary chain, the one not

Please cite this article in press as: Turk et al., The structure-function relationship of a signaling-competent, dimeric Reelin fragment, Structure (2021), https://doi.org/10.1016/j.str.2021.05.012

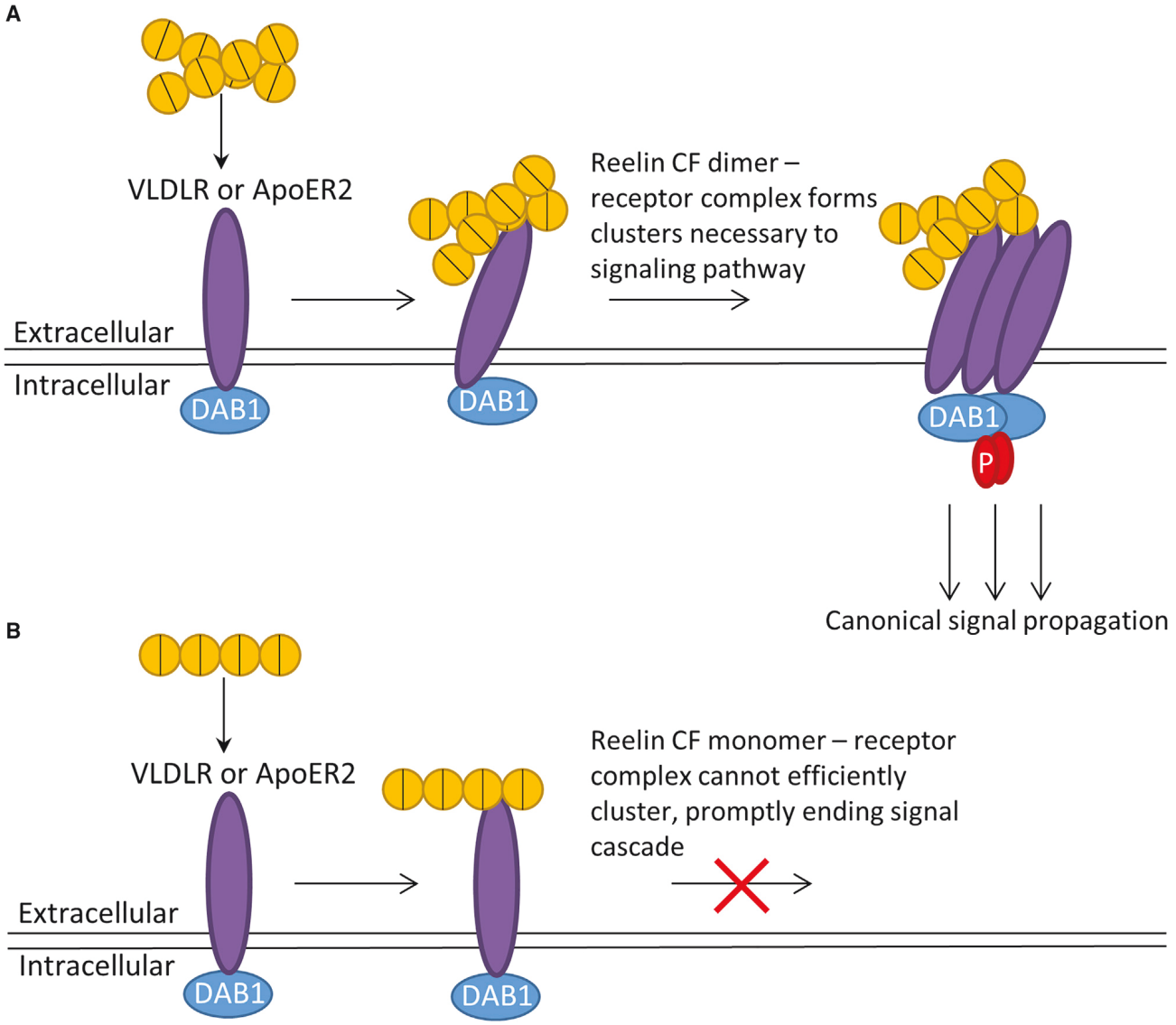

Figure 9. Suggested mode of dimeric activation

(A) X-like architecture enables the Reelin CF dimer to bind to either ApoER2 or VLDLR, forming a distinct Reelin-receptor complex in a conformation that favors receptor clustering to initiate canonical pathway signaling.

(B) Reelin CF monomer binds to VLDLR or ApoER2, but is unable to form an active Reelin-receptor complex that can efficiently cluster and activate the signal cascade.

directly binding to the receptor, plays a role in signal activation. Whether the secondary chain provides stability or interacts with the receptor after the initial binding event by K2467, identifying the domains (e.g., RR3 or RR4) needed on the secondary chain to create a signaling-competent dimer, may provide useful information to further understand this pathway.

STAR★METHODS

Detailed methods are provided in the online version of this paper and include the following:

- KEY RESOURCES TABLE
- RESOURCE AVAILABILITY
  - Lead contact
  - Materials availability
  - Data and code availability
- EXPERIMENTAL MODEL AND SUBJECT DETAILS
  - HEK293 cell culture
  - Primary neuronal cultures
- METHOD DETAILS
  - Protein expression and purification
  - Immunofluorescence and high-content analysis (HCA) of microscopy images
  - Western blot analysis of phosphorylation
  - mRNA isolation and quantitative reverse transcription PCR (RT-qPCR) analysis
  - Bio-layer interferometry

- Cryo-ET data collection and reconstruction
- Reelin CF dimer subtomogram classification and averaging
- Reelin CF monomer modeling
- Small angle scattering

- ANALYTICAL ULTRACENTRIFUGATION
- QUANTIFICATION AND STATISTICAL ANALYSIS

SUPPLEMENTAL INFORMATION

Supplemental information can be found online at https://doi.org/10.1016/j.str.2021.05.012.

ACKNOWLEDGMENTS

This work was funded in part by the National Science Foundation, award 1755189, by the Wellington Medical Research Foundation, 2019/301, and via strategic research funds from the School of Biological Sciences at Victoria University of Wellington to D.C.; NIGMS T32 GM008339 to L.S.T.; and RWJ Foundation grant 74260 to the Child Health Institute of New Jersey. This work was also funded by National Science Foundation award 1755184 to G.D. and by a Rutgers Busch Biomedical Research Grant to W.D. We acknowledge partial funding support for R.C.J.D. and M.J.C. from The Royal Society Marsden Fund (UOC1506).

We thank Jason Kaelber at Rutgers CryoEM & Nanoimaging Facility for his support in data collection. We acknowledge the Cornell High Energy Synchrotron Source (Ithaca, NY). CHESS is supported by NSF award DMR-1829070, and the MacCHESS resource is supported by NIGMS award 1-P30-GM124166-01A1 and NYSTAR. We would also like to thank Dr. Jill Trewhella for helpful discussions on the SAXS data interpretation.

AUTHOR CONTRIBUTIONS

D.C., G.D., and W.D. conceived the study. D.C. and L.S.T. designed, conducted, and analyzed the SAXS experiments. L.S.T., K.P., and D.M. were responsible for the production of purified Reelin fragments for all experiments in the manuscript. W.D. and X.K. designed and performed the cryo-ET experiments; W.D., M.C., and K.H. analyzed the cryo-ET data. G.D., K.P., V.D.P., and L.S.T. designed and performed the neuronal culture experiments. M.J.C., L.S.T., and R.C.J.D. designed, performed, and analyzed the AUC experiments. D.C., G.D., W.D., and L.S.T. performed overall data interpretation and co-wrote the manuscript. All authors read and discussed the manuscript.

DECLARATION OF INTERESTS

The authors declare no competing interests.

Received: February 9, 2021
Revised: April 26, 2021
Accepted: May 14, 2021
Published: June 4, 2021

REFERENCES

Ballif, B.A., Arnaud, L., and Cooper, J.A. (2003). Tyrosine phosphorylation of Disabled-1 is essential for Reelin-stimulated activation of Akt and Src family kinases. Brain Res. Mol. Brain Res. *117*, 152–159.

Bock, H.H., Jossin, Y., Liu, P., Forster, E., May, P., Goffinet, A.M., and Herz, J. (2003). Phosphatidylinositol 3-kinase interacts with the adaptor protein Dab1 in response to Reelin signaling and is required for normal cortical lamination. J. Biol. Chem. *278*, 38772–38779.

Bock, H.H., and May, P. (2016). Canonical and non-canonical reelin signaling. Front. Cell. Neurosci. *10*, 166.

Borrell, V., Del Rio, J.A., Alcantara, S., Derer, M., Martinez, A., D'Arcangelo, G., Nakajima, K., Mikoshiba, K., Derer, P., Curran, T., et al. (1999). Reelin regulates the development and synaptogenesis of the layer-specific entorhino-hippocampal connections. J. Neurosci. *19*, 1345–1358.

Brookes, E., Cao, W., and Demeler, B. (2010). A two-dimensional spectrum analysis for sedimentation velocity experiments of mixtures with heterogeneity in molecular weight and shape. Eur. Biophys. J. *39*, 405–414.

Brookes, E., and Demeler, B. (2007). Parsimonious regularization using genetic algorithms applied to the analysis of analytical ultracentrifugation experiments. In Proceedings of the 9th Annual Conference on Genetic and Evolutionary Computation, pp. 361–368.

Chen, M., Bell, J.M., Shi, X., Sun, S.Y., Wang, Z., and Ludtke, S.J. (2019). A complete data processing workflow for cryo-ET and subtomogram averaging. Nat. Methods *16*, 1161–1168.

D'Arcangelo, G., Homayouni, R., Keshvara, L., Rice, D.S., Sheldon, M., and Curran, T. (1999). Reelin is a ligand for lipoprotein receptors. Neuron *24*, 471–479.

D'Arcangelo, G., Miao, G.G., Chen, S.C., Soares, H.D., Morgan, J.I., and Curran, T. (1995). A protein related to extracellular matrix proteins deleted in the mouse mutant reeler. Nature *374*, 719–723.

D'Arcangelo, G., Nakajima, K., Miyata, T., Ogawa, M., Mikoshiba, K., and Curran, T. (1997). Reelin is a secreted glycoprotein recognized by the CR-50 monoclonal antibody. J. Neurosci. *17*, 23–31.

Dai, W., Fu, C., Raytcheva, D., Flanagan, J., Khant, H.A., Liu, X., Rochat, R.H., Haase-Pettingell, C., Piret, J., Ludtke, S.J., et al. (2013). Visualizing virus assembly intermediates inside marine cyanobacteria. Nature *502*, 707–710.

Del Rio, J.A., Heimrich, B., Borrell, V., Forster, E., Drakew, A., Alcantara, S., Nakajima, K., Miyata, T., Ogawa, M., Mikoshiba, K., et al. (1997). A role for Cajal-Retzius cells and reelin in the development of hippocampal connections. Nature *385*, 70–74.

Demeler, B. (2010). Methods for the design and analysis of sedimentation velocity and sedimentation equilibrium experiments with proteins. Curr. Protoc. Protein Sci. *7*, Unit 7 13.

Divekar, S.D., Burrell, T.C., Lee, J.E., Weeber, E.J., and Rebeck, G.W. (2014). Ligand-induced homotypic and heterotypic clustering of apolipoprotein E receptor 2. J. Biol. Chem. *289*, 15894–15903.

Dlugosz, P., Tresky, R., and Nimpf, J. (2019). Differential action of reelin on oligomerization of ApoER2 and VLDL receptor in HEK293 cells assessed by time-resolved anisotropy and fluorescence lifetime imaging microscopy. Front. Mol. Neurosci. *12*, 53.

Franke, D., Petoukhov, M.V., Konarev, P.V., Panjkovich, A., Tuukkanen, A., Mertens, H.D.T., Kikhney, A.G., Hajizadeh, N.R., Franklin, J.M., Jeffries, C.M., et al. (2017). Atsas 2.8: a comprehensive data analysis suite for small-angle scattering from macromolecular solutions. J. Appl. Crystallogr. *50*, 1212–1225.

Hiesberger, T., Trommsdorff, M., Howell, B.W., Goffinet, A., Mumby, M.C., Cooper, J.A., and Herz, J. (1999). Direct binding of Reelin to VLDL receptor and ApoE receptor 2 induces tyrosine phosphorylation of disabled-1 and modulates tau phosphorylation. Neuron *24*, 481–489.

Hirota, Y., and Nakajima, K. (2017). Control of neuronal migration and aggregation by reelin signaling in the developing cerebral cortex. Front. Cell Dev. Biol. *5*, 40.

Hopkins, J.B., Gillilan, R.E., and Skou, S. (2017). BioXTAS RAW: improvements to a free open-source program for small-angle X-ray scattering data reduction and analysis. J. Appl. Crystallogr. *50*, 1545–1553.

Howell, B.W., Herrick, T.M., and Cooper, J.A. (1999). Reelin-induced tyrosine [corrected] phosphorylation of disabled 1 during neuronal positioning. Genes Dev. *13*, 643–648.

Iafrati, J., Orejarena, M.J., Lassalle, O., Bouamrane, L., Gonzalez-Campo, C., and Chavis, P. (2014). Reelin, an extracellular matrix protein linked to early onset psychiatric diseases, drives postnatal development of the prefrontal cortex via GluN2B-NMDARs and the mTOR pathway. Mol. Psychiatry *19*, 417–426.

Jossin, Y., and Goffinet, A.M. (2007). Reelin signals through phosphatidylinositol 3-kinase and Akt to control cortical development and through mTor to regulate dendritic growth. Mol. Cell Biol. *27*, 7113–7124.

Jossin, Y., Ignatova, N., Hiesberger, T., Herz, J., Lambert de Rouvroit, C., and Goffinet, A.M. (2004). The central fragment of Reelin, generated by proteolytic

processing in vivo, is critical to its function during cortical plate development. J. Neurosci. *24*, 514–521.

Koie, M., Okumura, K., Hisanaga, A., Kamei, T., Sasaki, K., Deng, M., Baba, A., Kohno, T., and Hattori, M. (2014). Cleavage within Reelin repeat 3 regulates the duration and range of the signaling activity of Reelin protein. J. Biol. Chem. *289*, 12922–12930.

Kubo, K., Mikoshiba, K., and Nakajima, K. (2002). Secreted Reelin molecules form homodimers. Neurosci. Res. *43*, 381–388.

Lambert de Rouvroit, C., de Bergeyck, V., Cortvrindt, C., Bar, I., Eeckhout, Y., and Goffinet, A.M. (1999). Reelin, the extracellular matrix protein deficient in reeler mutant mice, is processed by a metalloproteinase. Exp. Neurol. *156*, 214–217.

Lambert de Rouvroit, C., and Goffinet, A.M. (1998). The reeler mouse as a model of brain development. Adv. Anat. Embryol. Cell Biol. *150*, 1–106.

Laue, T., Shah, B., Ridgeway, T., and Pelletier, S.L. (1992). Computer-Aided Interpretation of Sedimentation Data for Proteins. In Analytical Ultracentrifugation in Biochemistry and Polymer Science, S.E. Harding., J.C. Horton., and A.J. Rowe., eds. (Royal Society of Chemistry), pp. 90–125.

Lee, G.H., Chhangawala, Z., von Daake, S., Savas, J.N., Yates, J.R., 3rd, Comoletti, D., and D'Arcangelo, G. (2014). Reelin induces Erk1/2 signaling in cortical neurons through a non-canonical pathway. J. Biol. Chem. *289*, 20307–20317.

Lee, G.H., and D'Arcangelo, G. (2016). New insights into reelin-mediated signaling pathways. Front. Cell. Neurosci. *10*, 122.

Liu, W.S., Pesold, C., Rodriguez, M.A., Carboni, G., Auta, J., Lacor, P., Larson, J., Condie, B.G., Guidotti, A., and Costa, E. (2001). Down-regulation of dendritic spine and glutamic acid decarboxylase 67 expressions in the reelin haploinsufficient heterozygous reeler mouse. Proc. Natl. Acad. Sci. U S A *98*, 3477–3482.

Lussier, A.L., Weeber, E.J., and Rebeck, G.W. (2016). Reelin proteolysis affects signaling related to normal synapse function and neurodegeneration. Front. Cell. Neurosci. *10*, 75.

Mastronarde, D.N. (1997). Dual-axis tomography: an approach with alignment methods that preserve resolution. J. Struct. Biol. *120*, 343–352.

Mastronarde, D.N. (2005). Automated electron microscope tomography using robust prediction of specimen movements. J. Struct. Biol. *152*, 36–51.

Matsuki, T., Matthews, R.T., Cooper, J.A., van der Brug, M.P., Cookson, M.R., Hardy, J.A., Olson, E.C., and Howell, B.W. (2010). Reelin and stk25 have opposing roles in neuronal polarization and dendritic Golgi deployment. Cell *143*, 826–836.

Nagae, M., Suzuki, K., Yasui, N., Nogi, T., Kohno, T., Hattori, M., and Takagi, J. (2020). Structural studies of reelin N-terminal region provides insights into a unique structural arrangement and functional multimerization. J. Biochem. mvaa144. https://doi.org/10.1093/jb/mvaa144.

Nichols, A.J., and Olson, E.C. (2010). Reelin promotes neuronal orientation and dendritogenesis during preplate splitting. Cereb. Cortex *20*, 2213–2223.

Niu, S., Renfro, A., Quattrocchi, C.C., Sheldon, M., and D'Arcangelo, G. (2004). Reelin promotes hippocampal dendrite development through the VLDLR/ApoER2-Dab1 pathway. Neuron *41*, 71–84.

Niu, S., Yabut, O., and D'Arcangelo, G. (2008). The Reelin signaling pathway promotes dendritic spine development in hippocampal neurons. J. Neurosci. *28*, 10339–10348.

Nogi, T., Yasui, N., Hattori, M., Iwasaki, K., and Takagi, J. (2006). Structure of a signaling-competent reelin fragment revealed by X-ray crystallography and electron tomography. EMBO J. *25*, 3675–3683.

Ogawa, M., Miyata, T., Nakajima, K., Yagyu, K., Seike, M., Ikenaka, K., Yamamoto, H., and Mikoshiba, K. (1995). The reeler gene-associated antigen on Cajal-Retzius neurons is a crucial molecule for laminar organization of cortical neurons. Neuron *14*, 899–912.

Ogino, H., Hisanaga, A., Kohno, T., Kondo, Y., Okumura, K., Kamei, T., Sato, T., Asahara, H., Tsuiji, H., Fukata, M., et al. (2017). Secreted metalloproteinase ADAMTS-3 inactivates reelin. J. Neurosci. *37*, 3181–3191.

Olson, E.C., Kim, S., and Walsh, C.A. (2006). Impaired neuronal positioning and dendritogenesis in the neocortex after cell-autonomous Dab1 suppression. J. Neurosci. *26*, 1767–1775.

Park, T.J., and Curran, T. (2008). Crk and Crk-like play essential overlapping roles downstream of disabled-1 in the Reelin pathway. J. Neurosci. *28*, 13551–13562.

Petoukhov, M.V., and Svergun, D.I. (2005). Global rigid body modeling of macromolecular complexes against small-angle scattering data. Biophys. J. *89*, 1237–1250.

Pettersen, E.F., Goddard, T.D., Huang, C.C., Couch, G.S., Greenblatt, D.M., Meng, E.C., and Ferrin, T.E. (2004). UCSF Chimera–a visualization system for exploratory research and analysis. J. Comput. Chem. *25*, 1605–1612.

Qiu, S., Korwek, K.M., Pratt-Davis, A.R., Peters, M., Bergman, M.Y., and Weeber, E.J. (2006). Cognitive disruption and altered hippocampus synaptic function in Reelin haploinsufficient mice. Neurobiol. Learn. Mem. *85*, 228–242.

Ranaivoson, F.M., Turk, L.S., Ozgul, S., Kakehi, S., von Daake, S., Lopez, N., Trobiani, L., De Jaco, A., Denissova, N., Demeler, B., et al. (2019). A proteomic screen of neuronal cell-surface molecules reveals IgLONs as structurally conserved interaction modules at the synapse. Structure *27*, 893–906 e899.

Ranaivoson, F.M., von Daake, S., and Comoletti, D. (2016). Structural insights into reelin function: present and future. Front. Cell Neurosci. *10*, 137.

Rice, D.S., Nusinowitz, S., Azimi, A.M., Martinez, A., Soriano, E., and Curran, T. (2001). The reelin pathway modulates the structure and function of retinal synaptic circuitry. Neuron *31*, 929–941.

Sato, Y., Kobayashi, D., Kohno, T., Kidani, Y., Prox, J., Becker-Pauly, C., and Hattori, M. (2016). Determination of cleavage site of Reelin between its sixth and seventh repeat and contribution of meprin metalloproteases to the cleavage. J. Biochem. *159*, 305–312.

Strasser, V., Fasching, D., Hauser, C., Mayer, H., Bock, H.H., Hiesberger, T., Herz, J., Weeber, E.J., Sweatt, J.D., Pramatarova, A., et al. (2004). Receptor clustering is involved in Reelin signaling. Mol. Cell. Biol. *24*, 1378–1386.

Turk, L.S., Mitchell, D., and Comoletti, D. (2020). Purification of a heterodimeric Reelin construct to investigate binding stoichiometry. Eur. Biophys. J. *49*, 773–779.

Turk, M., and Baumeister, W. (2020). The promise and the challenges of cryo-electron tomography. FEBS Lett. *594*, 3243–3261.

Wasser, C.R., and Herz, J. (2017). Reelin: neurodevelopmental architect and homeostatic regulator of excitatory synapses. J. Biol. Chem. *292*, 1330–1338.

Weeber, E.J., Beffert, U., Jones, C., Christian, J.M., Forster, E., Sweatt, J.D., and Herz, J. (2002). Reelin and ApoE receptors cooperate to enhance hippocampal synaptic plasticity and learning. J. Biol. Chem. *277*, 39944–39952.

Yasui, N., Kitago, Y., Beppu, A., Kohno, T., Morishita, S., Gomi, H., Nagae, M., Hattori, M., and Takagi, J. (2011). Functional importance of covalent homodimer of reelin protein linked via its central region. J. Biol. Chem. *286*, 35247–35256.

Yasui, N., Nogi, T., Kitao, T., Nakano, Y., Hattori, M., and Takagi, J. (2007). Structure of a receptor-binding fragment of reelin and mutational analysis reveal a recognition mechanism similar to endocytic receptors. Proc. Natl. Acad. Sci. U S A *104*, 9988–9993.

Yasui, N., Nogi, T., and Takagi, J. (2010). Structural basis for specific recognition of reelin by its receptors. Structure *18*, 320–331.

Please cite this article in press as: Turk et al., The structure-function relationship of a signaling-competent, dimeric Reelin fragment, Structure (2021), https://doi.org/10.1016/j.str.2021.05.012

STAR★METHODS

KEY RESOURCES TABLE

REAGENT or RESOURCE	SOURCE	IDENTIFIER
Antibodies		
Rabbit IgG anti-AKT	Cell Signaling	Cat# 4961
Mouse IgG anti-FLAG® (DYKDDDDK)	Sigma	Cat# F3165
Rabbit IgG anti-phosphoAKT (Ser473)	Cell Signaling	Cat# 9271
Rabbit IgG anti-phosphoAKT (Thr308)	Cell Signaling	Cat# 9275
Mouse IgG2a anti- βIII TUBULIN (TuJ1)	Bio Legend	Cat# MMS-435P
Mouse IgG anti-GAD67	Millipore	Cat# MAB5406
Mouse IgG anti-GFAP	Dako	Cat# 20334
Mouse IgG2b anti-HuCD	Thermofisher	Cat# A-21271
Rabbit IgG anti-MAP2	Millipore	Cat# AB5622
Mouse IgG anti-NeuN	Millipore	Cat# MAB377
Rabbit IgG anti-phosphoS6 (Ser235/236) Alexa Fluor 488-conjugated	Cell Signaling	Cat# 4803
Goat anti-mouse IgG HRP	Invitrogen	Cat# G-21040
Goat anti-mouse IgG Cyanine5	Invitrogen	Cat# A10524
Goat anti-rabbit IgG HRP	Santa Cruz	Cat# SC-2004
Chemicals, peptides, and recombinant proteins		
DMEM	Thermo Fisher Scientific	Cat# SH30022FS
FBS	Atlanta Biologicals	Cat# S11550
G418 (Geneticin)	Sigma	Cat# 108321-42-2
Expi293™ expression medium	Gibco	Cat# A1435101
HRV-3C protease	This paper	N/A
B-27™ Plus Neuronal Culture System	Gibco	Cat# A3653401
FLAG® Peptide	Sigma	Cat# F3290
Polyethylenimine (PEI)	Fisher	Cat# NC9197339
L-Glutamine	Cytiva	Cat# SH30034.01
Poly-D-lysine	Sigma	Cat# P0899
cOmplete protease inhibitor	Roche	Cat# 46931590001
PhosSTOP	Roche	Cat# 4906845001
FLAG-Reelin CF	This paper	N/A
FLAG-Reelin NT	This paper	N/A
FLAG-Reelin CT	This paper	N/A
FLAG-Reelin FL	This paper	N/A
FLAG-Reelin CF C2101A	This paper	N/A
FLAG/His6-Reelin HD-Fc	Turk et al., 2020.	N/A
FLAG-Reelin CF-Fc	This paper	N/A
His6-Reelin CF K2467A-Fc	This paper	N/A
FLAG-ApoER2-Fc	This paper	N/A
FLAG-VLDLR-Fc	This paper	N/A
Critical commercial assays		
Papain dissociation kit	Worthington	Cat# LK003150
RNeasy Kit	Qiagen	Cat# 74104
Power SYBR Green master mix	Applied Biosystems	Cat# 4367659
QuikChange II XL Site-Directed Mutagenesis Kit	Agilent	Cat# 200521

(*Continued on next page*)

Please cite this article in press as: Turk et al., The structure-function relationship of a signaling-competent, dimeric Reelin fragment, Structure (2021), https://doi.org/10.1016/j.str.2021.05.012

Continued

REAGENT or RESOURCE	SOURCE	IDENTIFIER
Deposited data		
Dimeric Reelin central fragment	This paper	EMDB ID: EMD-23091
Crystal structure of two repeat fragment of Reelin	Yasui et al., 2007	PDB ID: 2E26
Crystal structure of the third repeat domain of Reelin	Nogi et al., 2006	PDB ID: 2DDU
Structural basis for specific recognition of Reelin by its receptors	Yasui et al., 2010	PDB ID: 3A7Q
Experimental models: cell lines		
HEK293 cells	ATCC	CRL-1573
HEK293S GnTI- cells	ATCC	CRL-3022
Expi293F™ cells	Gibco	Cat# A14635
Experimental models: Organisms/strains		
C57BL/6 primary mouse cortical neurons	Gibco	Cat# A15586
CD-1 mice	Charles River Laboratory	Strain code: 022
Oligonucleotides		
C2101A forward5'-gaaacgcacagatc cagcaaggtgcagctttccgaagt-3'	IDT	N/A
C2101A reverse5'-acttcggaaagct gcaccttgctggatctgtgcgtttc-3'	IDT	N/A
K2467A forward5'-gcccaggtctgctgcgcgt caaaaggcgctgg-3'	IDT	N/A
K2467A reverse5'-ccagcgccttttgac gcgcagcagacctgggc-3'	IDT	N/A
c-Fos forward5'-cgggtttcaacgccgacta-3'	IDT	N/A
c-Fos reverse5'-ttggcactagaga cggacaga-3'	IDT	N/A
Arc forward 5'-aagtgccgagctgagatg-3'	IDT	N/A
Arc reverse 5'-cgacctgtgcaacccttc-3'	IDT	N/A
S12 forward 5'-ggcatagctgctggaggtgtaa-3'	IDT	N/A
S12 reverse 5'-gggcttggcgcttgtctaa-3'	IDT	N/A
Recombinant DNA		
pCMV6-XL4 FLAG-RELN-Fc	Lee et al., 2014	N/A
pCMV6-XL4 FLAG-RELN CF-Fc	Lee et al., 2014	N/A
pCMV6-XL4 His6-RELN CF-Fc	This paper	N/A
pCMV6-XL4 FLAG-RELN NT-Fc	Ranaivoson et al., 2019	N/A
pCMV6-XL4 FLAG-RELN CT-Fc	Ranaivoson et al., 2019	N/A
pCMV6-XL4 FLAG-APOER2-Fc	Ranaivoson et al., 2019	N/A
pCMV6-XL4 FLAG-VLDLR-Fc	Ranaivoson et al., 2019	N/A
pCMV6-XL4 FLAG-RELN CF C2101A-Fc	This paper	N/A
pCMV6-XL4 His6-RELN CF K2467A-Fc	This paper	N/A
Software and algorithms		
Chimera	Pettersen et al., 2004	https://www.cgl.ucsf.edu/chimera/
ATSAS 3.0.0 software package (incl. Primus, DAMMIN, DAMAVER, DAMFILT)	Franke et al., 2017	https://www.embl-hamburg.de/biosaxs/download.html
BioXTAS RAW	Hopkins et al., 2017	https://bioxtas-raw.readthedocs.io/en/latest/

(*Continued on next page*)

Please cite this article in press as: Turk et al., The structure-function relationship of a signaling-competent, dimeric Reelin fragment, Structure (2021), https://doi.org/10.1016/j.str.2021.05.012

Continued

REAGENT or RESOURCE	SOURCE	IDENTIFIER
SASREF	Petoukhov and Svergun. 2005	https://www.embl-hamburg.de/biosaxs/sasref.html
UltraScanIII	Demeler, 2010	http://ultrascan.aucsolutions.com/
EMAN2	Chen et al., 2019	https://blake.bcm.edu/emanwiki/EMAN2
IMOD	Mastronarde, 1997	https://bio3d.colorado.edu/imod/
Prism 8	GraphPad	https://www.graphpad.com/
IN Carta Image Analysis	Molecular Devices	https://www.moleculardevices.com/products/cellular-imaging-systems/acquisition-and-analysis-software/in-carta-image-analysis-software#gref
Other		
Superose 6 Increase 10/300 GL	Cytiva	Cat# 29-0915-96
HiLoad 16/600 Superdex 200 PG	Cytiva	Cat# 28989335
Protein-A Sepharose fast flow resin	Cytiva	Cat# 17127902
anti-FLAG® M2 affinity gel	Sigma	Cat# A2220
Profinity™ IMAC Ni-charged resin	Bio-Rad	Cat# 156-0133
An-50 Ti Analytical 8-Place Titanium Rotor	Beckman Coulter	Cat# 363782
An-60 Ti Analytical 4-Place Titanium Rotor	Beckman Coulter	Cat# 361964
6 nm fiducial gold	EMS	Cat# 25510
Quantifoil R 2.0/1.0 Cu 200 mesh grids	EMS	Cat# Q2100CR1

RESOURCE AVAILABILITY

Lead contact

Further information and requests for resources and reagents should be directed to and will be fulfilled by the lead contact, Davide Comoletti (davide.comoletti@vuw.ac.nz).

Materials availability

Plasmids, cell lines, and recombinant proteins generated in this study are available upon request to the lead contact.

Data and code availability

The accession number for the electron density map of the dimeric Reelin central fragment reported in this paper is EMDB: EMD-23091.

EXPERIMENTAL MODEL AND SUBJECT DETAILS

HEK293 cell culture

HEK293 or HEK293S GntI- cells were cultured in DMEM supplemented with 5% fetal bovine serum (FBS) at 37°C and 5% CO_2. When culturing stable cell lines, HEK293 cells were maintained in DMEM supplemented with 5% FBS and 500 μg/ml of G418 at 37°C and 5% CO_2.

Expi293F™ cells were cultured in Expi293™ Expression Medium (Gibco) at 37°C and 8% CO_2 while shaking at 125 rpm.

Primary neuronal cultures

Cerebral cortices were dissected from the brains of E16 mice of the CD-1 strain and dissociated using papain (Worthington) in HBSS buffer supplemented with 1 M EDTA and 0.5 M $CaCl_2$. Cells were plated in 24-well plates at 1 x 10^5 cells/well for immunofluorescence experiments or in 6-well plates at 5 x 10^6 cells/well for Western blotting. For the neuronal culture involving the Reelin CF heterodimer, frozen, dissociated primary mouse cortical neurons (Gibco) were thawed and plated in 24-well plates at 1 x 10^5 cells/well. All plates were coated with poly-D-lysine and cells were cultured in Neurobasal medium supplemented with 2% B-27 supplement and 0.5 mM L-glutamine to promote neuronal growth and survival. Cells were cultured for 4-10 DIV in a 37°C tissue culture incubator.

METHOD DETAILS

Protein expression and purification

FL, NT, CT, and CF *Reelin* cDNA were cloned into a modified pCMV6-XL4 vector in frame with an N-terminal FLAG or His6 tag and C-terminal human Fc fragment (Lee et al., 2014; Ranaivoson et al., 2019). The C2101A and K2467A mutations were introduced using site-directed mutagenesis (Agilent) and were sequence confirmed.

Please cite this article in press as: Turk et al., The structure-function relationship of a signaling-competent, dimeric Reelin fragment, Structure (2021), https://doi.org/10.1016/j.str.2021.05.012

Stable cell lines were made for all Reelin constructs. HEK293 cells were transfected with the cDNA encoding the gene of interest as well as one empty vector (pcDNA3.1) fostering resistance against G418 using the Calcium Phosphate method. Cells were selected in DMEM supplemented with 5% FBS and 500 μg/ml of G418. Resistant clones were isolated using Pyrex cloning rings (Corning) and stable expression of the proteins were tested via western blot. Clones that highly expressed the protein were amplified, frozen, and used in large-scale protein production.

Proteins were fused to the Fc region of human IgG and secreted into the cell culture medium. Large-scale protein production was performed in Nunc™ TripleFlask™ cell culture flasks with regular collection and replenishment of the cell culture medium containing 2-5% FBS. Secreted proteins were purified via affinity chromatography, captured on Protein-A Sepharose 4 fast flow resin (Cytiva). The saturated resin was washed (50 mM Tris pH 7.4, 450 mM NaCl), equilibrated (50 mM Tris pH 7.4, 150 mM NaCl, 1 mM DTT), and the protein was eluted (50 mM Tris pH 7.4, 150 mM NaCl, 1 mM DTT, 10 μg/ml HRV-3C protease) by cleaving the protein at an HRV-3C protease site engineered between the C-terminal of the protein and the start of the Fc region. The eluted protein was then concentrated to an appropriate volume using Vivaspin concentrators (Sartorius-Stedim) and further purified via size exclusion chromatography using either a Superose 6 Increase 10/300 GL or a HiLoad 16/600 Superdex 200 PG column (Cytiva) equilibrated in 20 mM HEPES pH 7.4, 150 mM NaCl, 1 mM $CaCl_2$). The protein samples were further concentrated and used immediately or flash-frozen in liquid nitrogen and stored at -80°C until needed.

The cDNA encoding the extracellular domains (ectodomains) of VLDLR and ApoER2 were cloned into the same pCMV6-XL4 vector as described above. Expi293F™ cells were transfected with the cDNA encoding the genes for the receptors using polyethylenimine (PEI). The cells expressing the Fc-fused receptors were kept at 37°C and 8% CO_2 with shaking for 4–5 days in Expi293™ Expression Medium before harvesting. Expression was tested by western blot, detecting the N-terminal FLAG tag.

To purify full fusion proteins in cases when it was beneficial to maintain the Fc tag (e.g. BLI experiments where the Fc tag was required to immobilize the protein to the biosensor and to maintain the dimeric conformation of Reelin without multiple rounds of size exclusion chromatography), the proteins were expressed as described above. However, the secreted proteins were purified via affinity chromatography, using anti-FLAG® M2 affinity resin (Sigma). The saturated resin was washed (50 mM Tris pH 7.4, 450 mM NaCl), equilibrated (50 mM Tris pH 7.4, 150 mM NaCl), and the protein was eluted (50 mM Tris pH 7.4, 150 mM NaCl, FLAG® peptide 100 μg/ml). The eluted protein was then concentrated to an appropriate volume using Vivaspin concentrators (Sartorius-Stedim) and used immediately or flash-frozen in liquid nitrogen and stored at -80°C until needed.

The Reelin CF heterodimer was purified as previously outlined (Turk et al., 2020). In short, the conditioned medium of HEK293 cells stably expressing both FLAG-Reelin CF-Fc and His6-Reelin CF K2467A-Fc was collected and purified in tandem using IMAC Ni^{2+} and anti-FLAG® M2 affinity resins. The IMAC Ni^{2+} resin was washed three times with 50 mM Tris pH 8.0, 150 mM NaCl, and 5 mM imidazole, and the protein was eluted using 50 mM Tris pH 8.0, 150 mM NaCl, and 400 mM imidazole. The resulting eluate was then incubated with the anti-FLAG resin for 2 hours, and the resin was washed three times with 50 mM Tris pH 8.0, 150 mM NaCl and eluted using 50 mM Tris pH 7.4, 150 mM NaCl, FLAG® peptide 100 μg/ml.

Immunofluorescence and high-content analysis (HCA) of microscopy images

DIV4 cortical neurons were exposed to each Reelin protein for 30 min (triplicate wells/treatment group), and then fixed in 4% paraformaldehyde (PFA), permeabilized with 0.1% Triton X-100 for 20 min and incubated with blocking buffer (5% normal goat serum in 0.1% Triton-X-100 in PBS) for 1 h at room temperature. A negative control (purified Reelin elution buffer) and a positive control (10% fetal calf serum) were included in each plate. Cells were incubated with primary antibodies at 4°C overnight followed by secondary antibodies (when needed) conjugated to AlexaFluor 647 (Table S1) and Hoechst stain solution (ThermoFisher) for 1 h at room temperature. Cells were then washed twice with PBS and imaged at 10x magnification using an automated confocal fluorescence microscope (INCell Analyzer 6500, Cytiva). For HCA we collected at random 9 images/well from 3 wells/group (27 images per treatment group corresponding to at least 1,000 cells per well). The data were analyzed using INCell Workstation or IN Carta software (Molecular Devices) to calculate the percentage of positive cells or the intensity of the antibody signal in each treatment group. Statistical analysis was conducted using the GraphPad Prism8 software (San Diego, CA, USA). Outliers identified with the ROUT test (Q = 1%) were eliminated from the analysis. The data were analyzed first for normal distribution using the Shapiro–Wilk test (=0.05); since the distribution was normal, the values were further analyzed by ordinary one-way ANOVA followed by Tukey's multiple comparison tests. Differences were considered statistically significant when $p \leq 0.05$.

Western blot analysis of phosphorylation

DIV4 cortical neurons were lysed in RIPA buffer (50 mM Tris pH 7.4, 1% NP-40, 0.25% deoxycholate, 150 mM NaCl, 1 mM EGTA) supplemented with protease inhibitor (cOmplete, Roche) and phosphatase inhibitor (PhosSTOP, Roche), and cleared by centrifugation at 3000 × *g* for 5 min at 4°C. Protein lysates were loaded onto 8% SDS-PAGE gels and transferred to nitrocellulose membranes. After transfer, the membranes were rinsed in water two times, incubated with Revert 700 total protein stain for 5 min, rinsed twice with wash solution and detected in the 700 nm channel using the Odyssey Fc Imaging System (LI-COR Biosciences). The membranes were washed in water and blocked in 3% nonfat dry milk for 1 hr before incubation with primary antibodies against phospho-Akt Ser473, phospho-Akt Thr308, and total Akt (Table S1) overnight. The membranes were then washed 3 times in Tris buffer saline with 0.1% tween (TBST), incubated for 1 hr with IRDye 800CW goat anti-rabbit IgG secondary antibodies (LI-COR catalog # 926–32,211) at room temperature and the density of protein bands was determined using the Odyssey Fc Imaging System (LI-COR Biosciences). The ratio of phospho/total Akt was determined from 2 independent experiments.

Please cite this article in press as: Turk et al., The structure-function relationship of a signaling-competent, dimeric Reelin fragment, Structure (2021), https://doi.org/10.1016/j.str.2021.05.012

mRNA isolation and quantitative reverse transcription PCR (RT-qPCR) analysis

DIV10 cortical neuronal cultures were exposed to Reelin proteins or control buffer for 2 hr. The total RNA was purified using the Qiagen (Hilden, Germany) RNeasy Kit and transcribed into cDNA using a High-Capacity cDNA Reverse Transcription kit (Applied Biosystems, Foster City, CA, USA). The resulting cDNA was analyzed by RT-qPCR using the Power SYBR Green master mix (Applied Biosystems, Foster City, CA, USA). The expression levels of *Arc* and *c-Fos* genes were analyzed using Applied Biosystems Real-Time PCR machines and the QuantStudio Design&Analysis V1.4.3 software. Gene expression values were first normalized to the ribosomal protein S12 (internal control) and then were further normalized to the average value of buffer control samples. Primers were: *c-Fos* forward (5′-CGGGTTTCAACGCCGACTA-3′), *c-Fos* reverse (5′-TTGGCACTAGAGACGGACAGA-3′), *Arc* forward (5′-AAGTGCCGAGCTGAGATG-3′), Arc reverse (5′-CGACCTGTGCAACCCTTTC-3′), *S12* forward (5′-GGCATAGCTGCTGGAGGTG-TAA-3′), and *S12* reverse (5′-GGGCTTGGCGCTTGTCTAA-3′). Data points represent the average of 2 replicate wells/group from $n = 3$ experiments. Statistical analysis was conducted using the GraphPad Prism8 software. The data were analyzed first for normal distribution using the Shapiro–Wilk test (=0.05); since distribution was normal, the values were further analyzed by ordinary one-way ANOVA followed by Tukey's multiple comparison tests. Differences were considered statistically significant when $p \leq 0.05$.

Bio-layer interferometry

BLI experiments were performed at room temperature on a BLItz instrument (ForteBio, Menlo Park, CA). Protein A biosensors were pre-wetted in 400 μL of 20 mM HEPES pH 7.4, 150 mM NaCl, 1 mM $CaCl_2$, 0.2% Tween 20, 0.1% bovine serum albumin (BSA) for 10 min before use. The Protein A biosensors were then incubated for 4–10 min to load the appropriate purified Fc-fusion protein (ecto-ApoER2 or ecto-VLDLR). The binding event took place in a 4 μL drop of purified protein at a series of concentrations, under agitation. The lengths of the association and dissociation steps were determined empirically so that signal returned to baseline when possible. When sensible, the BLI experiments were performed in triplicate or duplicate. For all BLI experiments, except that between VLDLR-Fc and Reelin CF C2101A, the association buffer was 20 mM HEPES pH 7.4, 150mM NaCl, 1 mM $CaCl_2$, 0.2% Tween 20, 0.1% BSA and the dissociation buffer was 20 mM HEPES pH 7.4, 150 mM NaCl, 1 mM EDTA, 0.2% Tween 20, 0.1% BSA. For the interaction between VLDLR-Fc and Reelin CF C2101A, both association and dissociation buffers were 20 mM HEPES pH 7.4, 150 mM NaCl, 1 mM $CaCl_2$, 0.2% Tween 20, 0.1% BSA. In cases when full dissociation was not possible (i. e. the signal did not return to baseline), individual Protein A biosensors were used for each concentration measured. The biosensors were incubated in equimolar solutions of the Fc-fusion protein for exactly 4 min before reading the baseline and measuring the association and dissociation phases. All aspects of the individually loaded BLI experiments were plotted and overlaid to ensure equal amounts of the Fc-fusion protein were immobilized to the biosensors (Figure S4). To determine a K_D, the maximum response at each concentration was plotted and fit using a one site – specific, nonlinear regression (GraphPad Prism8).

Cryo-ET data collection and reconstruction

Reelin CF monomer or dimer samples were first mixed with 6 nm gold particles (EMS), which serve as fiducial markers to facilitate tilt series alignment during data processing. An aliquot of 3.5 μL of sample was applied to glow discharged Quantifoil holey grids (Quantifoil R 2.0/1.0, Cu, 200 mesh, EMS) prior to vitrification using a Leica EM GP plunger (Leica microsystems). 2D projection images and tilt series of the samples were collected in a Talos Arctica cryo-electron microscope (Thermo Fisher Scientific) equipped with a post-column BioQuantum energy filter (the slit was set to 20 eV), a K2 direct electron detector, and Volta phase plates at the back focal plane. Tilt series of Reelin CF monomers and dimers were collected under low dose conditions at 49,000× microscope magnification with a pixel size of 2.78 A/pixel, at defocus close to −0.5 μm with Volta phase plate or −4 μm without phase plates. Automated data collection was performed using SerialEM (Mastronarde, 2005) under the following illumination settings: spot size 8, 100 μm condenser aperture and 100 μm objective aperture. Typically, a tilt series ranges from −60° to 60° at 3° step increments. The accumulated dose for each tilt series was 50–60 electrons/$Å^2$. Tilt series alignment and reconstruction were performed using IMOD (Mastronarde, 1997).

Reelin CF dimer subtomogram classification and averaging

Subtomogram processing was done using the latest EMAN2 tomography workflow (Chen et al., 2019). From tomograms of CF dimers, 7,729 subtomograms were extracted using a box size of 168^3 voxels. A reference-free initial model was generated from a small subset of particles and used for subtomogram refinement for the entire dataset. After aligning all particles to the initial model, particles were classified based on intrinsic structural features using a model-free alignment algorithm. The number of classes was determined by the overall structural heterogeneity of the dimer population, and by visual inspection of the class averages to ensure that each class average demonstrates significant structural variation compared to averages from all other classes. Classes of particles with weaker RR3 or RR6 densities were excluded in further structural analysis. For class averages obtained from the second iteration of subtomogram averaging, the angle between the two monomers, defined as the acute angle between the long axis of the two monomers, and the distance between the C-terminal ends of RR6 on each monomer were measured in UCSF Chimera (Pettersen et al., 2004). Particles from classes with similar angles and distances were combined, refined, and averaged to achieve the final subtomogram average. An X-ray crystallography structure of RR5-6 (PDB: 2E26) was used as the reference model and fitted into the four repeats of each monomer to map the dimerization site and the receptor binding regions on the average map of the dimers.

Please cite this article in press as: Turk et al., The structure-function relationship of a signaling-competent, dimeric Reelin fragment, Structure (2021), https://doi.org/10.1016/j.str.2021.05.012

Reelin CF monomer modeling

To model for CF monomer flexibility, subtomograms of monomers were extracted from 3D tomograms and bandpass filtered to reduce high frequency noises and low frequency gradients from ice thickness variations. Each repeat of the monomer was modeled as a 40 Å sphere positioned at the center of mass for each repeat. Neighboring repeats in the same monomer were connected by linkers. Visualization of individual subtomograms and their corresponding 3D models was done in UCSF Chimera.

Small angle scattering

Reelin's monomeric central fragment was purified and buffer exchanged in PBS pH 7.4 by size exclusion chromatography and the fraction corresponding to the main peak was collected as well as PBS from a nearby fraction to use as a blank. The protein was concentrated to 1.1 g/L, and SAXS data was collected at the G1 beamline at the Cornell High Energy Synchrotron Source (Ithaca, NY). Twenty exposures of one second each at 20°C were taken at both 1.1 g/L and 0.55 g/L. Data reduction and the initial quality assessment were performed using BioXTAS RAW (Hopkins et al., 2017), and the data was further analyzed using the ATSAS 3.0.0 software package (Franke et al., 2017).

P(r) was calculated using Primus (Franke et al., 2017). DAMMIN *ab initio* bead modeling generated independent models that were subsequently aligned, averaged and filtered using the DAMAVER and DAMFILT programs (Franke et al., 2017). Rigid body modeling was performed using SASREF (Petoukhov and Svergun, 2005).

ANALYTICAL ULTRACENTRIFUGATION

Sedimentation velocity AUC experiments were performed in a Beckman Optima XL-I at the University of Canterbury Biomolecular Interaction Center (Christchurch, New Zealand). Reelin CF samples were measured at 0.057 g/L, 0.18 g/L and 0.4 g/L (unfractionated samples), 0.29 g/L (monomer), 0.21 g/L (dimer) and 0.21 g/L (higher order species) (fractionated samples) and 0.1 g/L and 0.3 g/L (C2101A mutant samples) in 50 mM Tris pH 8, 150 mM NaCl, 1 mM $CaCl_2$. Experimental data were collected at 20°C; reference solution (buffer) and sample solutions were added to 12 mm double sector cells with quartz or sapphire windows. Samples were run in an An-50 or An-60 Ti rotor at 32,000 rpm and scanned at 280 nm (fractionated samples), 286 nm (unfractionated samples) or 290 nm (C2101A mutant samples). Data were analyzed with UltraScan-III v.4.0, release 5812. The partial specific volume of Reelin CF (0.726 mL/g) was estimated by UltraScan from protein sequence, analogous to methods outlined by Laue et al. (Laue et al., 1992). The influence of glycosylation on the partial specific volume was not considered as it was not necessary to be able to distinguish between a monomeric or dimeric particle. Data were analyzed using two-dimensional spectrum analysis and genetic algorithm-Monte Carlo analysis (Brookes et al., 2010; Brookes and Demeler, 2007; Demeler, 2010).

QUANTIFICATION AND STATISTICAL ANALYSIS

Statistical analysis was performed using the GraphPad Prism8 software and all information regarding this can be found within the appropriate figure legends, results section, and method details.